Larsen, H.C., Saunders, A.D., Clift, P.D., et al., 1994
Proceedings of the Ocean Drilling Program, Initial Reports, Vol. 152

12. SITE 919[1]

Shipboard Scientific Party[2]

HOLE 919A

Date occupied: 13 November 1993

Date departed: 14 November 1993

Time on hole: 21 hr, 40 min

Position: 62°40.20′N, 37°27.611′W

Bottom felt (drill-pipe measurement from rig floor, m): 2099.5

Distance between rig floor and sea level (m): 11.3

Water depth (drill-pipe measurement from sea level, m): 2088.2

Total depth (from rig floor, m): 2193.0

Penetration (m): 93.50

Number of cores (including cores having no recovery): 10

Total length of cored section (m): 93.5

Total core recovered (m): 93.59

Core recovery (%): 100.1

Oldest sediment cored:
Depth (mbsf): 93.5
Nature: silty clay
Age: Quaternary
Measured velocity (km/s): 1.75

HOLE 919B

Date occupied: 14 November 1993

Date departed: 14 November 1993

Time on hole: 12 hr, 55 min

Position: 62°40.201′N, 37°27.618′W

Bottom felt (drill-pipe measurement from rig floor, m): 2097.3

Distance between rig floor and sea level (m): 11.3

Water depth (drill-pipe measurement from sea level, m): 2086.0

Total depth (from rig floor, m): 2244.3

Penetration (m): 147.0

Number of cores (including cores having no recovery): 8

Total length of cored section (m): 75.7

Total core recovered (m): 77.28

Core recovery (%): 102.1

Oldest sediment cored:
Depth (mbsf): 147.0
Nature: silty clay
Age: Quaternary
Measured velocity (km/s): 1.67

Comments: Drilled from 18.7 to 90.0 mbsf.

HOLE 919C

Date occupied: 14 November 1993

Date departed: 15 November 1993

Time on hole: 1 day, 2 hr, 50 min

Position: 62°40.198′N, 37°27.625′W

Bottom felt (drill-pipe measurement from rig floor, m): 2097.3

Distance between rig floor and sea level (m): 11.3

Water depth (drill-pipe measurement from sea level, m): 2086.0

Total depth (from rig floor, m): 2157.4

Penetration (m): 60.1

Number of cores (including cores having no recovery): 0

Total length of cored section (m): 0

Total core recovered (m): 0

Core recovery (%): 0

Comments: Washed from 0 to 60.1 mbsf, but not cored.

Principal results: The sediment column at Site 919 has been assigned to one lithologic unit that is at least 147 m thick (Fig. 1). The dominant lithology comprises clay and silt in various proportions and nearly 200 distinct beds or packages of beds were identified in the sediment sequence. Many of the beds show fining-upward and sharp basal contacts, indicating deposition from turbidity currents. Other beds have more irregular contacts and more poorly sorted interiors, which may result from deposition from melting icebergs and subsequent reworking by mass flow, bottom currents, and bioturbation on the seafloor. Dropstones occur throughout the sediment column, but they are smaller and less frequent than those found at the other Leg 152 sites.

A variety of detrital grains occur in this sediment; quartz is ubiquitous. Commonly associated with quartz are amphibole, clinopyroxene, and opaque minerals. Other minerals include garnet, epidote, and sphene. Volcanic glass is a common constituent. Most of the mineral grains probably originate in Greenland; the volcanic detritus in Iceland. Discrete airfall volcanic ash layers occur at nine places in the cores.

Frequent seismic reflectors in the upper part of the sediment column at this site cannot be correlated with layers or structures in the observed cores.

The nannofossils recovered from Hole 919B indicate that the oldest sediment is of upper Pliocene age. An extended Quaternary sequence (about 93.5 m) has been recovered from Hole 919A. Planktonic assemblages are abundant and well preserved throughout. Siliceous microfossils, such as radiolarians and sponge spicules, are generally common to abundant.

The interval from 152-919A-1H, 0 cm, to -919B-6H-2, 35 cm, is dominantly of normal polarity, with two intervals comprising reversed and/or mixed polarity records. Below interval 152-919B-6H-2, 35 cm (121 mbsf), the sediment is reversely magnetized. The uppermost, normal polarity event can be correlated with the Brunhes Chron. However, the lowest part of the normal event is close to or within the Pliocene/Pleistocene boundary, suggesting that it must be the normal part of the Matuyama Event. This implies that the reversed polarity section of the upper part of the Matuyama Event is missing, and that an unconformity, of the order of 1 m.y., exists in the sequence. No evidence for such a hiatus can be seen, either in the lithostratigraphy or in the MST records.

[1] Larsen, H.C., Saunders, A.D., Clift, P.D., et al., 1994. *Proc. ODP, Init. Repts.*, 152: College Station, TX (Ocean Drilling Program).

[2] Shipboard Scientific Party is as given in the list of participants preceding the contents.

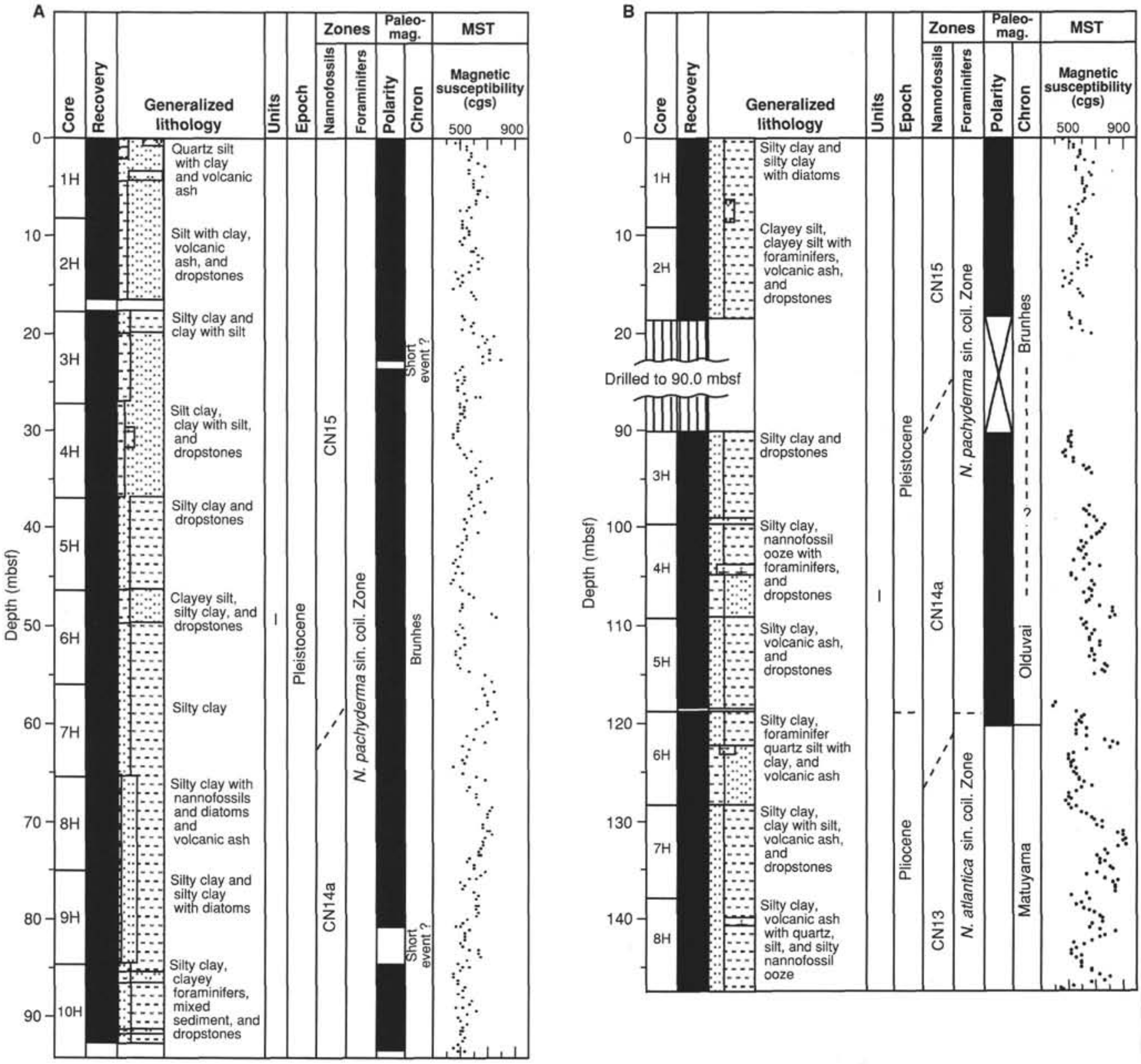

Figure 1. Site summary data for Site 919. **A.** Hole 919A. **B.** Hole 919B.

Seventy-two samples were analyzed for total organic carbon (TOC), nitrogen, sulfur, and inorganic carbon. Calcium carbonate content ranges from 0% to about 10%, with its concentration controlled by the abundances of planktonic foraminifers. Abundances of TOC, total nitrogen, and total sulfur are low. Total organic carbon/total nitrogen ratios indicate that the organic matter is predominantly marine. However, given the low TOC content, these ratios should be used cautiously. Methane concentrations are high (400–20,000 ppm) in the lower part of the sediment column (85 to 147 mbsf). In the upper part of the column, methane concentration is close to the detection limit of the equipment. The methane distribution curve is similar to that determined at Site 918.

Dense sampling of the Pleistocene sediment interstitial pore water was conducted to define seawater salinity distribution and to sharpen the boundary between the sulfate reduction and the methane production zones. Similar studies were conducted at Site 918, but in less detail. A well-developed chloride maximum of ≈572 mM occurs at ≈50 mbsf. From 20 to 90 mbsf, the concentration profile for sulfate is essentially linear with depth toward the base of the sulfate reduction zone. This suggests transport by diffusive exchange. Methane levels have been kept low, presumably by the action of sulfate-reducing bacteria.

MST and other physical properties were measured on all of the cores from Site 919, with the exception of Cores 152-919B-1H and -2H, which were analyzed by MST only. On the basis of the MST data, all of the sediments were grouped into one mechanical unit, which was subdivided on the basis of bulk density and *P*-wave velocity into three subunits (M1a, M1b and M1c). The patterns in the MST and physical properties data suggest that the sediment at Site 919 has experienced several changes in depositional environment, even though little variation is seen in lithology.

There is no evidence from the MST data to support the existence of an unconformity between about 120 and 125 mbsf, as inferred by the magnetostratigraphic and biostratigraphic data.

BACKGROUND AND SCIENTIFIC OBJECTIVES

Introduction

Site 919 is located in 2088.2 m of water on the continental rise of Southeast Greenland, within the western part of the Irminger Basin. This site is located at the seaward end of the proposed Site EG63 transect, at the position of the planned Site EG63-3 (see Figs. 5 and 6, "Introduction" chapter, this volume). The original objective of proposed Site EG63-3 was to drill through the approximately 1400-m-thick Cenozoic sediment cover and to recover the underlying oceanic basement, located on magnetic Chron C24n.1. At this site, it might be expected that the emplacement environment and the geochemical composition of the volcanic basement would reflect the change from formation of an SDRS to regular ocean crust. However, proposed Site EG63-3 was not scheduled to be drilled to basement during Leg 152. Thus, Site 919 (located at proposed Site EG63-3) was drilled as a contingency site, and as a result of limited time available, it had restricted objectives. These were as follows: (1) to provide high-resolution stratigraphic sampling of the presumably expanded, and compared to Site 918, more fine-grained and complete Quaternary section; and (2) to provide data for planning possible later, deep drilling into basement at this site.

No specific underway geophysical survey was done to locate Site 919. The position of the site was determined by coordinates from the preexisting site-survey data (see "Pre-cruise Site Surveys" chapter, this volume). The site is located at the intersection of high-resolution seismic Lines GGU/EG92-37 and GGU/EG92-39 (Fig. 2). The site lies close to the deep seismic Line GGU81-08, used during the original planning of Leg 152.

The seismic stratigraphic framework of the Quaternary to late Pliocene section at Site 919 is described briefly below and is followed by a description of the drilling results. Seismic reflection time has been converted to preliminary depth values using an average *P*-wave velocity of 1700 m/s.

Seismic Stratigraphy

Only the uppermost part of the thick sedimentary section is described here. One apparent seismic stratigraphic sequence is present between the seafloor and approximately 240 mbsf (280 ms TWT; Fig. 3). Its lower boundary is an unconformity, with the sequence below showing a different internal reflector pattern. However, at this stage, we have not formally defined seismic stratigraphic sequences for this site. It is conceivable that the top 240 mbsf (280 ms TWT) at Site 919 corresponds to Sequence 1 and the upper part of Sequence 2 at Site 918.

The seismic expression of the upper 280 ms (approximately 240 m) of the sedimentary column is uniform, with densely spaced (on the order of a few meters), parallel reflectors with extremely good continuity (Fig. 3). With only a few minor exceptions, the reflectors are concordant with the seafloor, which has a southerly dip of about 0.5°. Seismic stratigraphic unconformities, representing small intervals of nondeposition or minor erosion, are seen at a few levels, in particular on the dip profile of Line EG92-39 (Fig. 3). Truncations below the seismic unconformities (marked 1–4) may indicate minor erosional episodes. At Site 919, these reflectors are found at TWT depths below seafloor of 85 ms (70 mbsf), 175 ms (150 mbsf), 220 ms (190 mbsf), and 240 ms (210 mbsf). Onlapping from the northwest onto possible, faint seismic unconformities, is seen at two levels between Reflectors 1 and 2. At Site 919, these reflectors are at depths of 115 and 135 mbsf (135 and 160 ms TWT). Minor faulting has affected the sediments below Reflector 2.

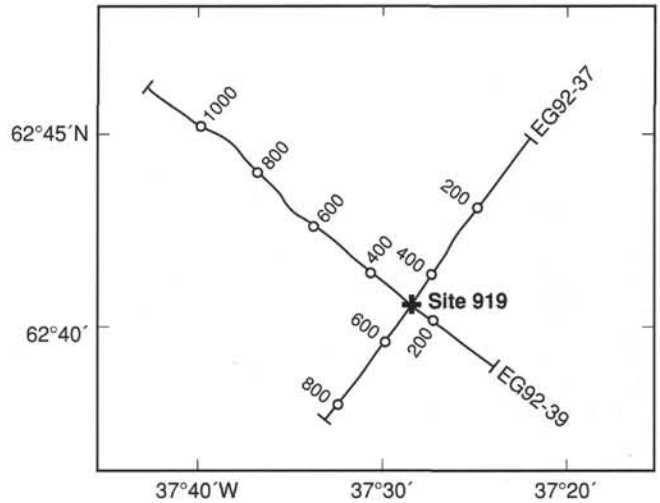

Figure 2. Location map of Site 919 (marked by a cross).

OPERATIONS

By 0215 hr on 13 November 1993, the vessel was under way at 6.4 kt to proposed Site EG63-3. Two extra persons were assigned to watch for ice on the bridge wings to ensure that any ice in the water would be avoided. Both spotlights were used to sweep the area in front of the vessel during the 40 nmi transit to the site. The vessel changed course once to avoid a large bergy bit.

Hole 919A

At 0800 hr on 13 November, a beacon was dropped on location (354B, 16.5 kHz, s.n. 763) following the short precision depth recorder survey of the area. By 0915 hr, the thrusters and hydrophones were lowered and the vessel was positioning over the beacon. From 0915 until 1045 hr, steam hoses had to be used to defrost the APC core barrels before they could be removed for use. Although antifreeze had been added to the storage shucks, no one had anticipated wind chills of minus 30°C, which had frozen the core barrels in place. The backup beacon (354B, 16 kHz, s.n. 752) was deployed at 1030 hr, when the initial beacon transmissions changed to half-pulsed rates.

A standard advanced piston core/extended core barrel (APC/XCB) bottom-hole assembly (BHA) was made up with a new Security S86F bit and then run into the hole to 2085.2 m below sea level (mbsl). At 1615 hr, Hole 919A was spudded with the first APC core, from which we recovered 8.02 m of clayey silt. This established the mudline depth at 2088.2 mbsl. The precision depth recorder had measured a depth of 2104.4 m. Table 1 records this and other coring information for Site 919.

After APC coring advanced from 0 to 93.5 mbsf (Cores 152-919A-1H to -10H), the core barrel for Core 152-919A-11H would not seat in the landing shoulder. Inspection of the cutting shoe revealed that the shoe had been brinelled in, suggesting a hard landing on the flapper. The only remaining option was to trip the BHA and inspect the lockable float valve (LFV). Operations in Hole 919A had cored 93.5 m and recovered 93.59 m (100.1%). The cores were oriented starting with Core 152-919A-4H.

The bit cleared the mud line at 0230 hr and was on deck at 0545 hr on 14 November. Inspection of the LFV revealed that the flapper hinge had parted and that the flapper was tightly jammed into the mouth of the LFV. The LFV was replaced, and the bit was run into the hole.

Hole 919B

After the vessel was offset 10 m to the south, APC-coring was resumed. At 1030 hr, the first mudline core of Hole 919B was ob-

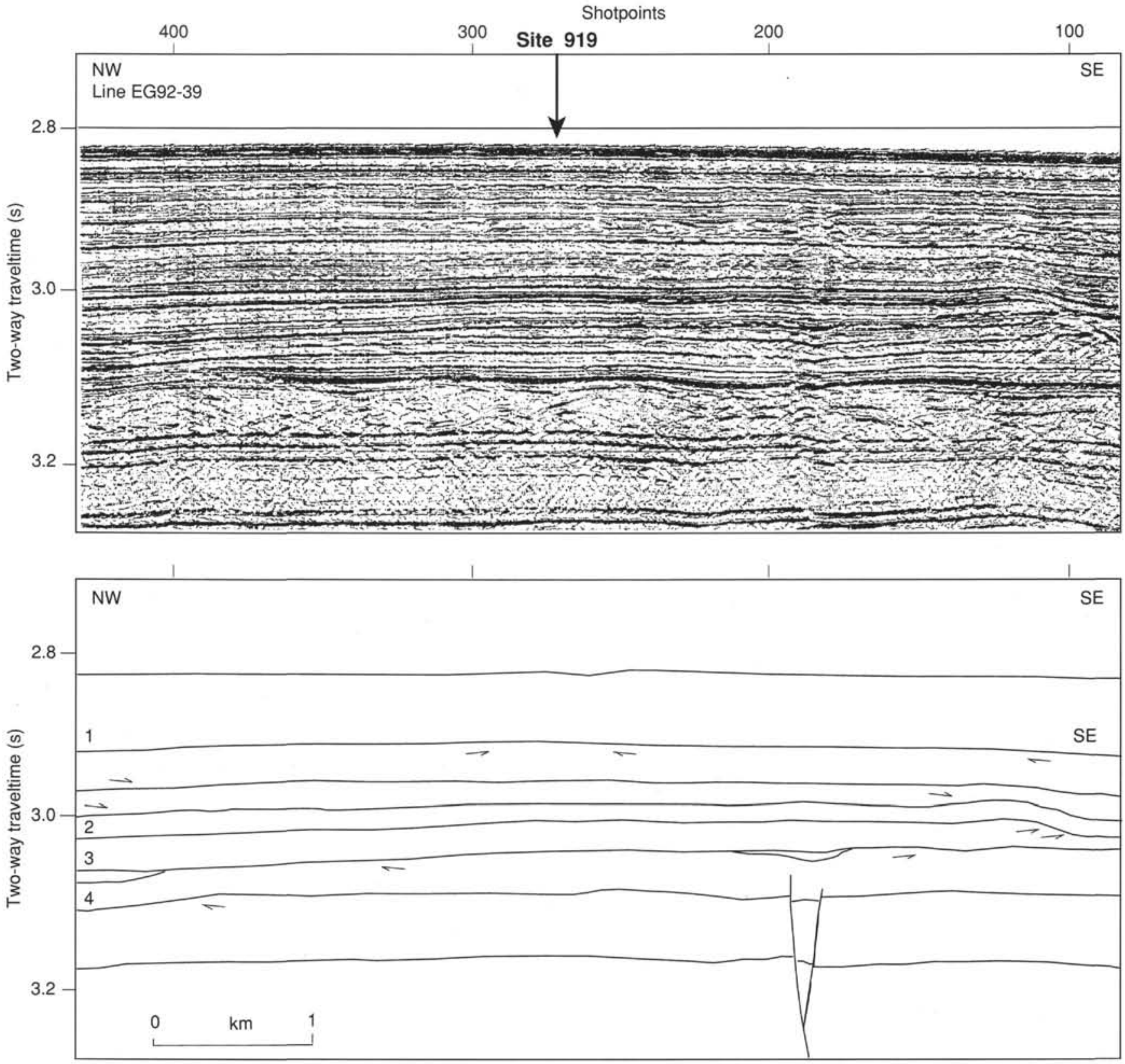

Figure 3. High-resolution seismic profile from Line EG92-39 through Site 919. Interpretation of the upper 300 ms (approximately 260 m) below the seafloor is shown in the line drawing. No formal seismic stratigraphic sequences have been defined. Reflectors 1 through 4 may represent erosional to nondepositional seismic unconformities. The interval from 0 to 280 ms below seafloor (0–250 mbsf) forms a seismically monotonous sequence. It is conceivable that it corresponds to seismic stratigraphic Sequence 1 and the upper part of Sequence 2 at Site 918.

tained and established the mudline depth at 2097.3 m (DPM). During APC-coring, drilling advanced from 0 to 18.7 m (Cores 152-919B-1H to -2H) and we recovered 18.67 m. The interval from 18.7 to 90.0 mbsf was washed ahead with a center bit and coring resumed. APC-coring advanced from 90.0 to 147.0 mbsf (Cores 152-919B-3H to -8H) to recover 58.61 m (103%), with Cores 152-919B-3H and below being oriented.

Meanwhile, an iceberg and a bergy bit, which had been closely watched, encroached upon the "Yellow" warning zone at 1.6 and 2.1 nmi, respectively. Coring operations were stopped while the bit was pulled out of the hole to 112.7 mbsf using the top drive. The top drive was set back, and the ice was observed as it approached our location. After waiting only 30 min, it was clear as the ice entered the "Red" warning zone that both bergs were headed directly toward the vessel location. The bit then was pulled above the mud line.

At 1840 hr, the vessel was offset in DP mode to starboard approximately 200 m. Both the iceberg and the bergy bit drifted directly over the location of Hole 919B. Meanwhile, a third iceberg (Number 84 of the cruise) was also being plotted and gave an indication of drifting toward our location. Concurrently with the appearance of the third iceberg, the weather began to deteriorate. By midnight of 14 November, winds were blowing at 42 kt from the north, with gusts up to 52 kt, and the barometer began to fall rapidly (981.0 mbar by midnight).

We spent the early morning hours of 15 November attempting to observe the iceberg as it approached our location using spotlights through the spray, growing swells, and snow. At 0145 hr, the iceberg passed within 0.4 nmi of our location, and the vessel was repositioned 10 m east of Hole 919B. A total of 8.5 hr was spent waiting for these three icebergs, not including any time spent tripping in and out of the hole related to ice movements.

Hole 919C

The center bit was dropped, and Hole 919C was spudded at 0145 hr on 15 November and then washed ahead to 60.1 mbsf. Our plan was to wash ahead to 140 mbsf and then to resume APC-coring, but this idea was thwarted when the weather worsened to storm force. At 0415 hr, the pipe was pulled above the mud line and we began to wait on the weather. Shortly after this, the storm increased to Force 12, with sustained winds of 60 kt and gusts up to 75 kt. The swells were 40 to 60 feet high, and green water was frequently breaking over the ship's bow. Acoustics were constantly being lost as a result of cavitation. The main propellers would overspeed as the stern of the vessel broke the surface. At this time, the lowest barometric pressure of the cruise was recorded (970.8 mbar).

At 0730 hr, a green wall of water cleared the main deck and passed around and over the bridge to slam against the starboard lifeboats and spray the drill floor. The starboard weather station was lost during this large wave. The vessel was unable to hold its location, but was able to maintain a heading into the wind as it was carried south.

A meeting was convened the morning of 15 November with the Co-Chiefs, the ODP Operations Superintendent, the SEDCO Drilling Superintendent, and the Captain to discuss the feasibility of staying in this area. All agreed that the constant presence of icebergs and the difficulty in detecting them in the lengthening dark hours and on radar, coupled with more frequent and intense storm activity, had made operations in the area unacceptably dangerous.

By 1400 hr on 15 November, the weather had improved to gale force, and the opportunity was taken to trip the pipe to the surface. The storm had taken the vessel 9 nmi south of the location of Hole 919C. By 2130 hr on 15 November, the BHA was broken into individual drill collars and laid down, and the vessel cautiously headed south. It was considered too dangerous to return to Site 919 to retrieve the two beacons.

Transit to St. John's

The vessel sailed at reduced speed through calm seas on 16 November. A Force 12 storm hit on the morning of 17 November, with sustained winds of 60 kt and gusts to 80 kt (highest recorded during the cruise) from 265°. Green water broke over the bow regularly, and one large wave inundated the bridge deck, damaged the starboard spotlight, and swept away the EPIRB beacon and life preserver stored on the starboard wing. A considerable amount of ship's motion was felt, and pitch and roll angles of 10° were common.

Numerous icebergs also were spotted visually and on radar throughout 17 November and were reported to the Canadian Ice Patrol in St. John's. The storm prevailed into the morning of 18 November, then gradually improved through the day.

LITHOSTRATIGRAPHY

Introduction

We drilled two holes at Site 919 (see "Operations" section, this chapter): Hole 919A (10 cores) was continuously cored to a depth of 93.5 mbsf and Hole 919B (eight cores) was cored and washed to a depth of 147 mbsf in two parts. An upper part (Cores 152-919B-1H and -2H) was cored to duplicate the top two cores of Hole 919A to recover two thin ash beds identified in Hole 919A. The remainder of Hole 919B was cored between depths of 90.0 and 147.0 mbsf (Cores 152-919B-3H through -8H). Recovery of sediment in the holes exceeds 100%. Combined, the two holes form a composite sequence 147 m thick.

Table 1. Coring summary, Site 919.

Core no.	Date (Nov. 1993)	Time (UTC)	Depth (mbsf)	Length cored (m)	Length recovered (m)	Recovery (%)
152-919A-						
1H	13	1725	0.0–8.0	8.0	8.02	100.0
2H	13	1755	8.0–17.5	9.5	8.46	89.0
3H	13	1830	17.5–27.0	9.5	9.86	104.0
4H	13	1930	27.0–36.5	9.5	9.86	104.0
5H	13	2000	36.5–46.0	9.5	9.77	103.0
6H	13	2045	46.0–55.5	9.5	9.83	103.0
7H	13	2130	55.5–65.0	9.5	9.81	103.0
8H	13	2215	65.0–74.5	9.5	9.78	103.0
9H	13	2300	74.5–84.0	9.5	9.88	104.0
10H	14	0010	84.0–93.5	9.5	8.32	87.6
Coring totals:				93.5	93.59	100.1
152-919B-						
1H	14	1150	0.0–9.2	9.2	9.26	100.0
2H	14	1230	9.2–18.7	9.5	9.41	99.0
		*** Drilled from 18.7 to 90.0 mbsf ***				
3H	14	1515	90.0–99.5	9.5	9.93	104.0
4H	14	1600	99.5–109.0	9.5	9.82	103.0
5H	14	1625	109.0–118.5	9.5	9.29	97.8
6H	14	1700	118.5–128.0	9.5	9.92	104.0
7H	14	1740	128.0–137.5	9.5	9.82	103.0
8H	14	1815	137.5–147.0	9.5	9.83	103.0
Coring totals:				75.7	77.28	102.1
152-919C-	***Washed from 0.0 to 60.1 mbsf. No coring.***					

We distinguished one lithologic unit at Site 919. Heterogeneities can be found within the sequence, but the observed features do not warrant division at this time.

Lithologic Units

Lithologic Unit I: silty clay, clayey silt, and clay with silt
Interval: Cores 152-919A-1H to -10H and 152-919B-1H to -8H
Depth: 0–147.0 mbsf
Thickness: 147.0 m
Age: Pleistocene and Pliocene

Sediment at Site 919 was assigned to one lithologic unit that is composed predominantly of silty clay, clayey silt, and clay with silt (Fig. 4). Sediments from the upper part, above a depth of about 20 mbsf, are somewhat coarser-grained than those lower in the section and consist of relatively more silt. Sediment from Site 919 generally is finer-grained than sediment from the upper Pliocene and Pleistocene sequences at Site 918.

The seismic reflection profile through Site 919 (see "Background and Scientific Objectives" section, this chapter) shows some relatively continuous, widely spaced reflectors in the upper part of the sedimentary section that can be traced laterally. The causes of the acoustic layering were not apparent from the lithological variations observed during our preliminary examination of the cores, nor did we see systematic variations in the physical properties of the sediment (see "Physical Properties" section, this chapter) that would explain the acoustic layering.

We were able to define nearly 200 separate beds and closely spaced combinations of beds by studying core photographs and visual core descriptions. These beds range in thickness from 5 cm to several meters. Most of the bedding is related to small changes in grain size and/or color. Many of the beds have fining-upward grain sizes and very sharp basal contacts, typical of transportation by, and deposition from, turbidity currents. Others have irregular top and bottom bedding contacts, and sorting is somewhat poorer than in the more coherent beds. We infer that some of these irregularities are related to deposition from the melting of sediment-rich pack ice and icebergs, combined with subsequent turbid flow along the seafloor.

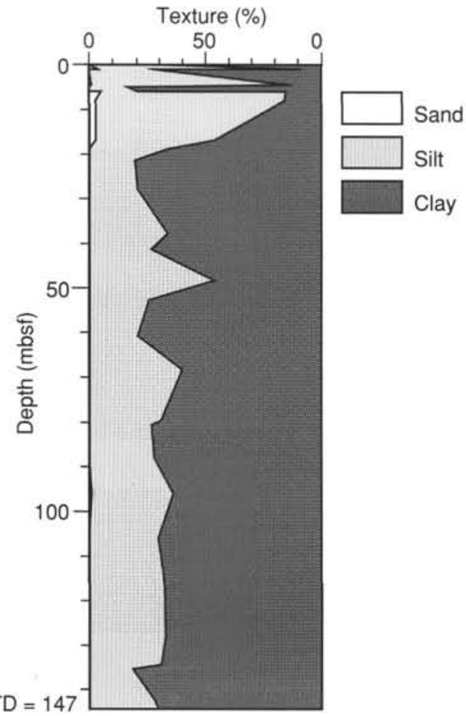

Figure 4. Grain-size distribution in lithologic Unit I, Holes 919A and 919B. Note the change from dominant silt (and sand) to dominant clay at about 20 mbsf.

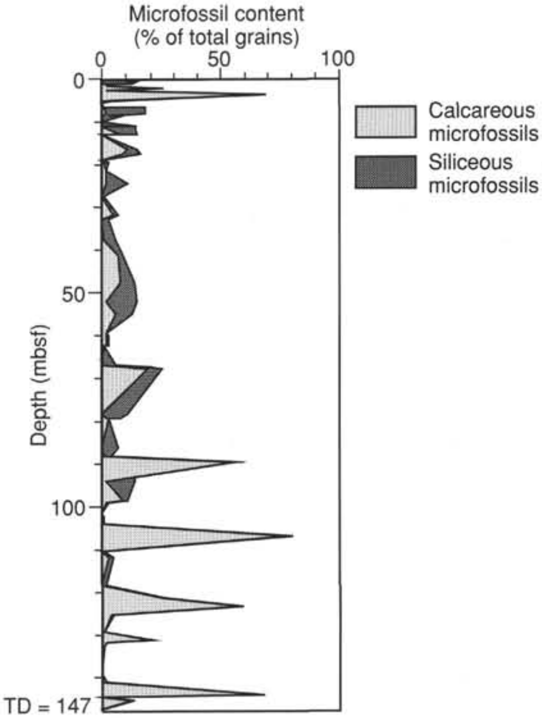

Figure 5. Siliceous (diatoms and sponge spicules) and calcareous (foraminifers, nannofossils, and micrite) microfossils in smear slides; Holes 919A and 919B. Compare with $CaCO_3$ contents (see "Organic Chemistry" section, this chapter). Below a depth of about 87 mbsf, diatom levels decline strongly.

The sediment varies in color from dark gray to dark brown to various hues of greenish gray. Some changes can be seen in the relative amounts of different colors downhole. For instance, to a depth of 58.5 mbsf, colors are predominantly dark gray and dark grayish-brown. Three thin greenish-gray intervals are located within that upper 58.5 m. Between 58.5 and 64.3 mbsf, four distinct, alternating sequences of dark gray and greenish-gray can be found. The interval between 64.3 and 120.5 mbsf is predominantly dark gray and dark grayish-brown. Greenish-gray packages of beds alternate with the darker gray and brown packages of beds between 120.5 mbsf and the bottom of the hole. These color changes may have been caused by cyclical changes in oceanographic conditions related to glaciation.

Biogenic components are dominated by diatoms, sponge spicules, and foraminifers, although in places, calcareous nannofossils are also important contributors (Fig. 5). Calcareous nannofossils are abundant over thin intervals within both the Pleistocene and Pliocene sediments, particularly in Sections 152-919A-8H-1 and -2 and Sections 152-919B-4H-4, -6H-1, and -8H-3. Diatoms are most abundant in the upper 87 m, and decrease below this level. Sponge spicules are common throughout the column, but are most abundant in the upper two cores of both holes.

Quartz is a ubiquitous component and is commonly associated with the accessory minerals amphibole (both metamorphic and volcanic), clinopyroxene, and opaque minerals. Garnet, epidote, and sphene occur in some smear slides. Volcanic glass is a common constituent. It is apparent that most of the nonbiogenic debris was derived from a continental source, probably East Greenland. Explosive volcanism, most likely in Iceland, contributed glass to the sediments.

Volcanic ash occurs at nine levels in the cores (Table 2; Figs. 6 and 7). Two ash beds in Core 152-919B-2H (Section 1, 107–108 cm, and Section 2, 26–27 cm) duplicate those in Core 152-919A-2H (Section 2, 141–142 cm, and Section 3, 18–21 cm), thereby making a total of 11 recovered ash layers and pods, but only nine discrete levels. The relatively high volcanic glass content in Interval 152-919A-1H-1, 0–30 cm, suggests that a young ash has been dispersed in the upper part of the core.

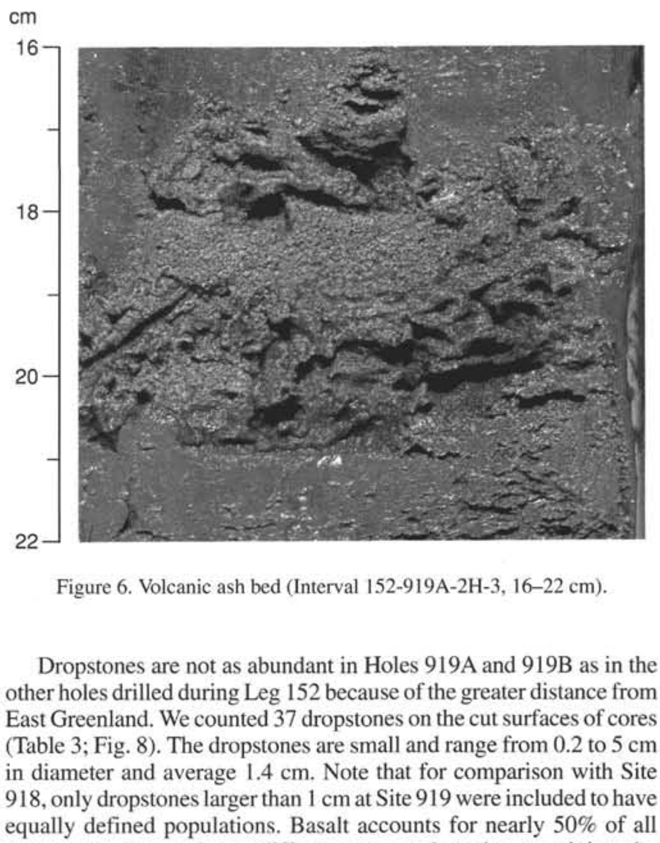

Figure 6. Volcanic ash bed (Interval 152-919A-2H-3, 16–22 cm).

Dropstones are not as abundant in Holes 919A and 919B as in the other holes drilled during Leg 152 because of the greater distance from East Greenland. We counted 37 dropstones on the cut surfaces of cores (Table 3; Fig. 8). The dropstones are small and range from 0.2 to 5 cm in diameter and average 1.4 cm. Note that for comparison with Site 918, only dropstones larger than 1 cm at Site 919 were included to have equally defined populations. Basalt accounts for nearly 50% of all dropstones, suggesting a different source than that supplying the glaciogenic sediments recovered at Sites 916 through 918.

Table 2. Volcanic ash beds in cores from Holes 919A and 919B.

Core, section, interval (cm)	Depth (mbsf)	Glass (%)	Remarks
152-919A-			
1H-1, 29–30	0.29	25	Dispersed in upper 30 cm.
2H-2, 141–142	10.91	60	Bed about 3 cm thick.
2H-3, 18–19	11.18	69	Contorted bed.
152-919B-			
2H-1, 107–108	10.27	89	Same as 152-919A-2H-2, 141 cm.
152-919A-			
2H-2, 26–27	10.96	95	Bed about 3 cm thick.
7H-4, 136–137	61.36	55	Black ash about 1 cm thick.
8H-1, 97–98	65.97	67	Small blebs.
10H-2, 105–106	86.55	55	Small black blebs.
152-919B-			
5H-5, 87–88	115.87	65	Black blebs.
6H-6, 89–90	126.89	55	Small distorted bed.
8H-3, 94–95	141.44	46	Clast 2 cm in diameter.

Table 3. Dropstones in Holes 919A and 919B.

Depth (mbsf)	Diameter (cm)	Gneiss	Met.	Basalt	Dolerite	Gabbro	Sed.	Unknown	Totals
2.00	5.00						1		1
5.26	3.00						1		1
7.80	1.20					1	1		2
11.61	1.50			1					1
22.38	1.5, 3.0	1	1						2
24.32	1.00			1					1
26.18	0.40			1					1
27.52	1.00			1					1
28.99	2.00			1					1
29.46	0.3, 0.3, 0.3			3					3
32.07	2.00				1				1
32.77	1.00						1		1
42.13	1.00			1					1
47.04	1.00	1							1
48.33	0.40			1					1
48.72	4.00	1							1
58.22	0.20							1	1
66.48	0.50							1	1
68.21	0.50							1	1
70.77	0.50							1	1
87.91	<0.4						1		1
87.96	<0.4						1		1
88.03	<0.4			1					1
91.35	1.40			1					1
92.16	<0.4						1		1
97.51	1.00							1	1
104.33	1.50			1					1
107.79	1.00			1					1
107.81	0.80	1							1
108.22	2.00			1					1
188.12	3.00			1					1
130.77	0.20								1
143.57	2.00			1					1

Note: Met. = metamorphic rocks other than gneiss, and Sed. = fine-grained siliciclastic rocks.

Some striking similarities exist between the sediment packages and beds in the upper cores from Holes 919A and 919B and those in the Pliocene and Pleistocene cores of lithologic Unit I at Site 918. For example, the small quartz-rich sediment stringers, quartz-rich pods, fining-upward quartz silt beds, and worm burrows filled with quartz silt are similar to those in Holes 918A and 918D, where they generally occur within greenish-gray beds. A few of the quartz silt beds exhibit channeling effects along the bottom contacts and graded beds that fine upward, thereby suggesting deposition from turbidity currents. Most of the small beds and laminae, however, show no internal features and probably are related to winnowing of the quartz grains by bottom currents.

Different sediments in the Irminger Basin are related to a wide variety of sedimentary processes. For example, the sediments in Holes 919A and 919B form a relatively homogeneous package on a large (tens of meters) scale, but at smaller (centimeters) scales, complexities related to differences in such factors as sediment transport

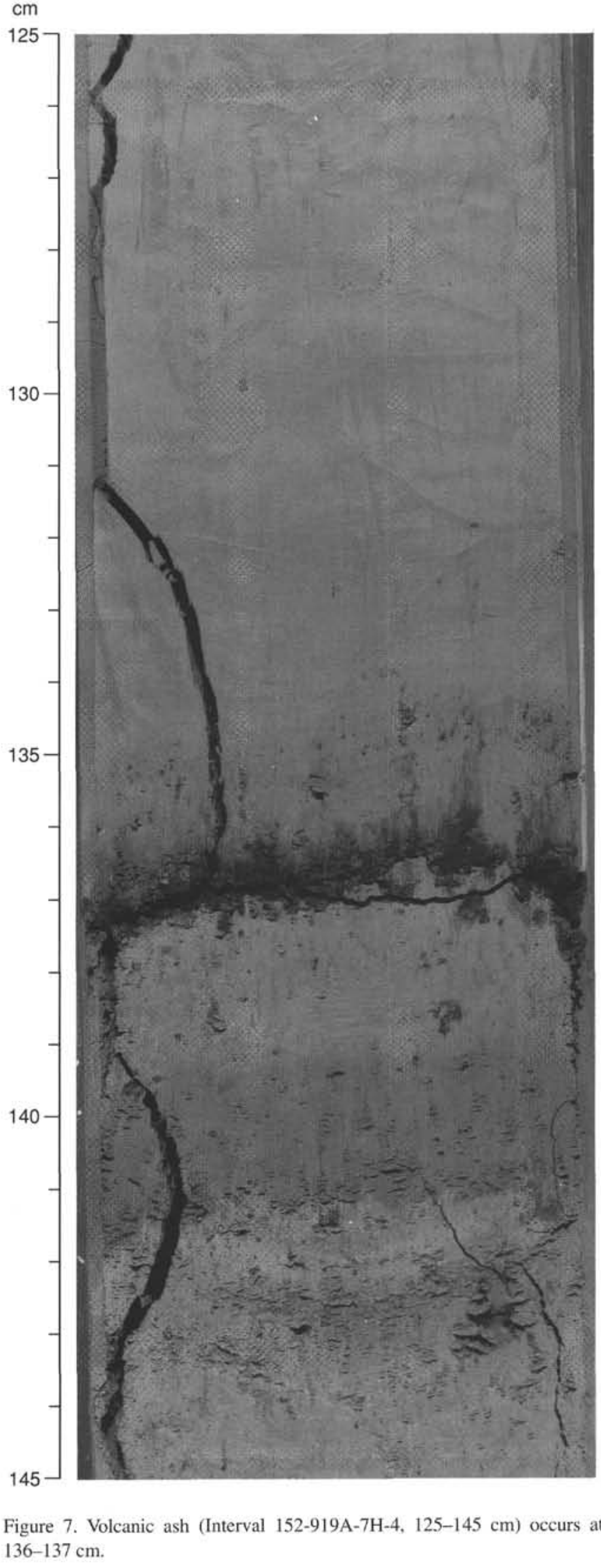

Figure 7. Volcanic ash (Interval 152-919A-7H-4, 125–145 cm) occurs at 136–137 cm.

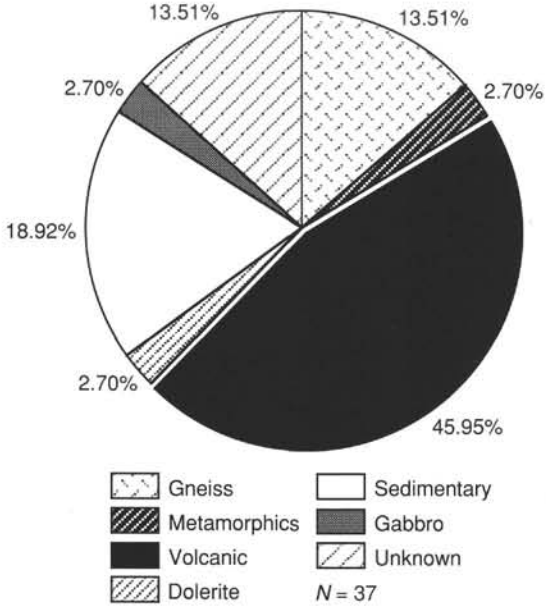

Figure 8. Diagram showing relative percentages of rock types in 37 dropstones (0.2–5 cm large) from Holes 919A and 919B.

mechanisms (e.g., turbidity currents, and bottom currents and droppings from melting icebergs), depositional environments (e.g., fan lobes, channels, abyssal plains), and overall compositional diversity of the sediment sources (e.g., relative percentages of biogenic components, volcanic ash, and terrigenous, or continentally derived, minerals) emerge. More complete interpretations must await shore-based mineralogic and biostratigraphic studies.

BIOSTRATIGRAPHY

Calcareous Nannofossils

The abundance of calcareous nannofossils varies from rare to abundant in the core-catcher samples from Site 919. Preservation of nannofossils is generally moderate. The lowest occurrence of *Emiliania huxleyi*, the biostratigraphic marker for the base of Zone CN15, has been tentatively placed below Sample 152-919A-6H-CC (55.5 mbsf), as it was difficult to identify this small species on board the ship (see discussion in "Biostratigraphy" section, "Site 918" chapter, this volume). The highest occurrence of *Pseudoemiliania lacunosa* is recorded in Sample 152-919A-7H-CC (65.0 mbsf); thus, the top of Subzone CN14a (0.45 Ma) can be drawn above this sample. The interval from 65.0 to 118.5 mbsf (Sample 152-919B-5H-CC) was placed in the middle to lower Pleistocene, on the basis of the occurrence of *P. lacunosa* and *Gephyrocapsa* spp. >4.0 µm. The interval from 128.0 mbsf (Sample 152-919B-6H-CC) to 147.0 mbsf (Sample 152-919B-8H-CC) has been assigned to the upper Pliocene, on the basis of the presence of *Calcidiscus macintyrei* and the absence of *Reticulofenestra gelida* (Figs. 9 and 10).

Planktonic Foraminifers

An extended Quaternary sequence of about 93.5 m was recovered in Hole 919A. Planktonic foraminiferal assemblages are abundant and well preserved throughout, whereas siliceous microfossils, such as radiolarians, diatoms, and sponge spicules, generally are common to abundant.

Neogloboquadrina pachyderma sinistral-coiling Zone was identified from Samples 152-919A-1H-CC to -10H-CC. Planktonic foraminiferal species generally include sinistrally coiled specimens of *N. pachyderma, G. glutinata, G. bulloides, T. quinqueloba*, along with rare *N. dutertrei, G. scitula*, and rarer *N. humerosa*. As the extinction of *N. humerosa* occurred during the early Pleistocene (Zone N22) according to Kennett and Srinivasan (1983), the occurrence of this species in Sample 152-919A-6H-CC suggests an early Pleistocene age for sediments below 55.5 mbsf.

Sample 152-919A-8H-CC contains, in addition to the previously mentioned species, a more diversified and apparently warmer-water assemblage that includes dextrally coiled specimens of *N. pachyderma, G. inflata, G. calida*, and *Globigerina* sp. A of Poore (1979).

The *Neogloboquadrina pachyderma* sinistral-coiling Zone was identified in the upper 118.5 m of sediment recovered at Hole 919B. In this zone, planktonic foraminiferal assemblages are generally moderately to well preserved, and siliceous microfossils, including radiolarians, diatoms, and sponge spicules, vary in abundance from rare to very abundant. The planktonic foraminiferal assemblage in Sample 152-919B-1H-CC is almost monospecific and consists of abundant sinistrally coiled specimens of *N. pachyderma*. Sample 152-919A-2H-CC contains a well-diversified assemblage that includes *N. pachyderma* sinistral-coiling, *G. bulloides, G. scitula, Globigerina rubescens, G. calida, T. quinqueloba, G. glutinata*, and rare *Globigerinita uvula*.

The sediment was washed from 18.7 to 90.0 mbsf in Hole 919B. Planktonic foraminiferal assemblages in Samples 152-919B-3H-CC to -5H-CC consist of common and moderately preserved sinistrally coiled specimens of *N. pachyderma, T. quinqueloba, G. juvenilis*, rare *N. dutertrei*, and *G. scitula*.

Neogloboquadrina pachyderma dextral-coiling Zone and *N. atlantica* dextral-coiling Zone of Spiegler and Jansen (1989) were not observed at Hole 919B.

Samples 152-919B-6H-CC to -8H-CC have been attributed to *N. atlantica* sinistral coiling Zone (Pliocene), based on the occurrence of sinistrally coiled specimens of *N. atlantica*. Species diversity in the Pliocene assemblages is higher than in the younger interval. These assemblages consist of sinistrally coiled specimens of *N. atlantica* and *N. pachyderma, G. bulloides, N. dutertrei, N. humerosa*, along with rare specimens of the temperate and warm-water species *G. scitula, G. inflata, H. riedeli*, and *Pulleniatina* spp. (Fig. 10).

Benthic Foraminifers

The benthic foraminiferal assemblages from all core-catcher samples (152-919A-1H-CC through -10H-CC and -919B-1H-CC through -8H-CC) were analyzed (Figs. 9 and 10). In general, the assemblages have been assigned to the *Cassidulina norvangi* assemblage previously described in the "Biostratigraphy" section, "Site 918" chapter (this volume).

Common and well-preserved benthic faunas, which constitute 5% to 15% of the total foraminiferal fauna, occur in Samples 152-919A-2H-CC, -7H-CC, and -9H-CC. *Astrononion gallowayi, C. norvangi, Cassidulina teretis, Cibicides refulgens*, and *Elphidium excavatum* are well represented in Sample 152-919A-2H-CC. In Sample 152-919A-7H-CC, *C. norvangi, C. teretis*, and *E. excavatum* are common. The benthic assemblage in Sample 152-919A-9H-CC includes common *E. excavatum* and *Buliminella elegantissima. Cassidulina teretis* was a dominant species during Pliocene to Pleistocene glacial intervals of the North Atlantic region (Murray, 1984). *Elphidium excavatum* also has been interpreted as being related to a glacial marine environment (Mackensen et al., 1985). Thus, benthic assemblages in Samples 152-919A-2H-CC, -7H-CC and -9H-CC suggest glacial conditions.

Sample 152-919A-4H-CC contains few and well-preserved benthic forms that contribute about 23% of the total foraminiferal fauna. *Bulimina aculeata* and *B. elegantissima* are common. The former species lives at a water depth of 1500 to 3000 m in the modern northeastern Atlantic (Murray, 1984). Therefore, this assemblage suggests a paleowater depth of 1500 to 3000 m.

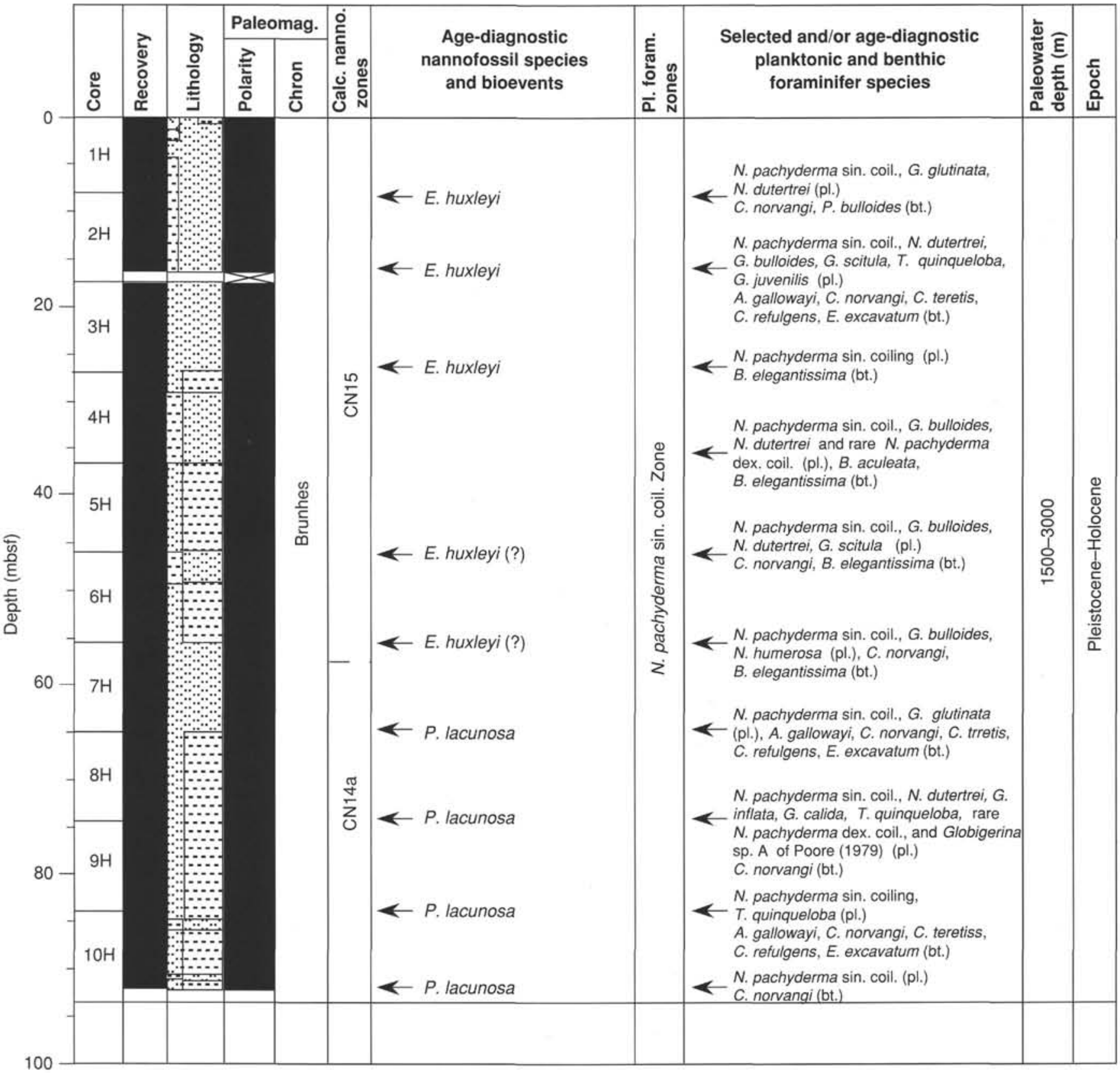

Figure 9. Biostratigraphic summary of Hole 919A. Paleowater depths inferred by benthic foraminiferal species also are shown. pl. = planktonic foraminifers, bt. = benthic foraminifers.

Scarce, moderately preserved benthic forms constitute about 10% of the total foraminiferal fauna in Sample 152-919B-6H-CC. *Pseudoparrella exigua* and *C. norvangi* are common. In the modern northeastern Atlantic, *Epistominella exigua* (= *P. exigua*) lives in a water depth deeper than 1500 m (Murray, 1984). The common occurrence of this species, therefore, indicates a paleowater depth deeper than 1500 m.

Sample 152-919B-7H-CC contains a few well-preserved benthic forms, that contribute about 5% of the total foraminiferal fauna. The assemblage includes common *Brizalina* sp., *Stainforthia fusiformis*, and *Oridorsalis umbonatus*. Because in the modern northeast Atlantic Ocean the latter species is distributed in water deeper than 1500 m (Murray, 1984), the assemblage in Sample 152-919B-7H-CC also suggests a paleowater depth deeper than 1500 m.

Biomagnetostratigraphic Correlation

Common *Calcidiscus macintyrei* and sinistrally coiled specimens of *Neogloboquadrina atlantica* are present from Sample 152-919B-6-CC down the hole. This suggests a late Pliocene age for this stratigraphic interval on the basis of biomagnetostratigraphic correlation established elsewhere, including that at nearby Site 918. This places constraints on the magnetostratigraphic interpretation at this site. Three interpretations are possible (Fig. 10):

1. The base of Brunhes is at 122 mbsf, and the reversely magnetized interval from the base of Cores 152-919B-6H through -8H is Chron 2r. This would suggest that most of Chron C1r and the entire C2n (Olduvai) are missing in the lower part of Core 152-919B-6H.

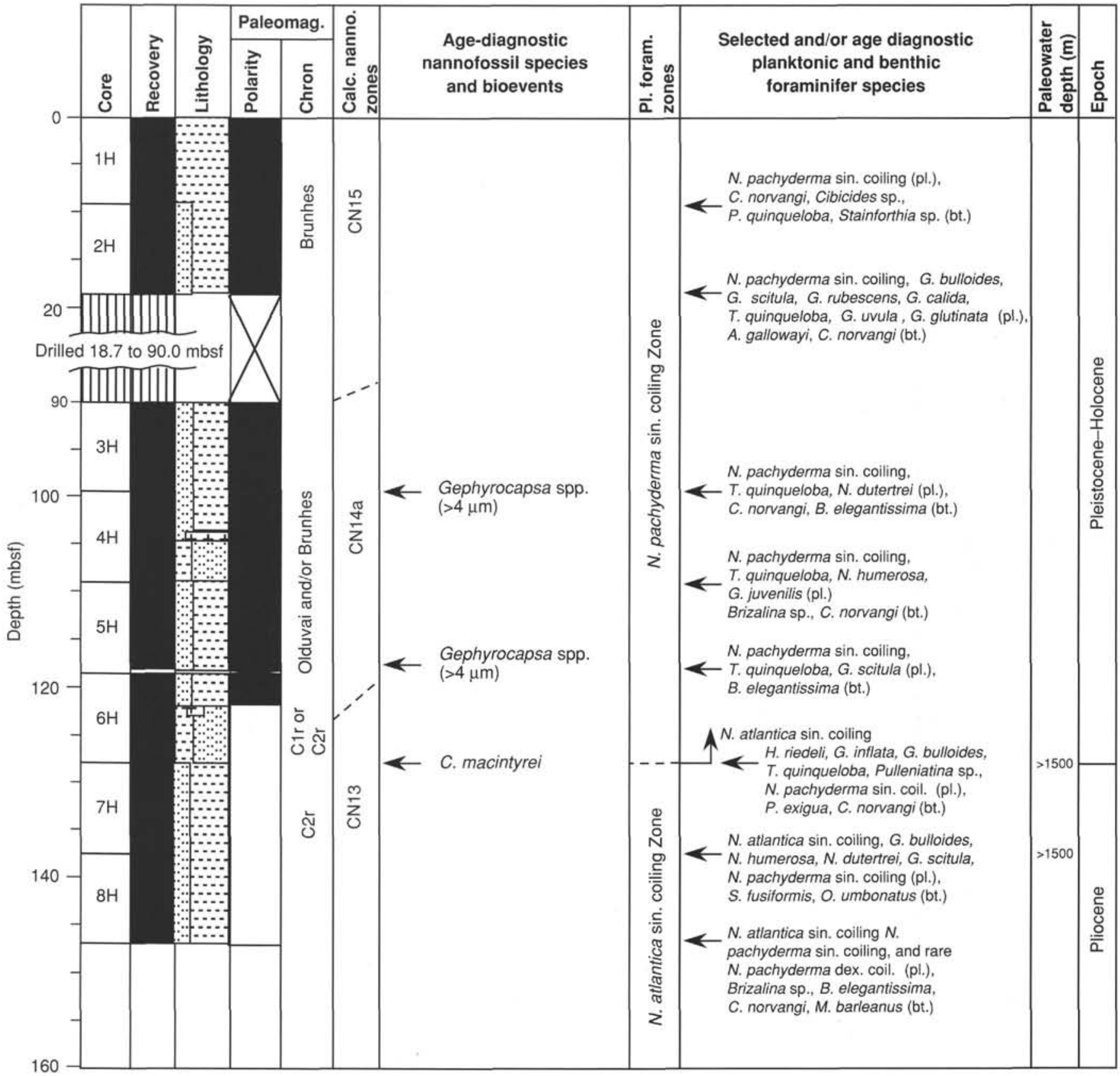

Figure 10. Biostratigraphic summary of Hole 919B. Paleowater depths inferred by benthic foraminiferal species also are shown. pl. = planktonic foraminifers, bt. = benthic foraminifers.

2. The base of Chron C2n is at 122 mbsf, and the reversely magnetized interval below is Chron C2r. This would suggest that the entire Chron C1r and possibly part of the lower Brunhes and upper Olduvai are missing above Core 152-919B-6H.

3. Chron C1r is present at Site 919, but is not identifiable on the basis of the shipboard magnetic data. This would suggest that no significant hiatuses exist. This interpretation would agree with the seismic data and sedimentation rate results (see "Sedimentation Rates" section, this chapter).

The first two interpretations are equally possible, although the third one is considered less likely based on evaluation of the magnetic polarity data. Detailed shore-based studies of biostratigraphy and magnetostratigraphy should help to determine where unconformities, if any, occur at Site 919.

PALEOMAGNETISM

The two holes drilled at Site 919 provide a 147-m composite section through upper Pliocene and Pleistocene sediments in the western Irminger Basin, southeast of Greenland. Holes 919A and 919B were drilled using the advanced piston coring (APC) technique, with recovery averaging 100.1% and 101.2%, respectively. Hole 919A penetrated 94.5 m of Pleistocene sediments. At Hole 919B, the interval between 0 and 18.7 mbsf was continuously cored (Cores 152-919B-1H and -2H) before the hole was washed down to 91.5 mbsf. Coring then recommenced to a total depth of 147 mbsf (Cores 152-919B-3H to -8H). Technical problems associated with the downhole operation of the Tensor tool mean that cores were not oriented with respect to the magnetic meridian.

Paleomagnetic studies were conducted on material from both Holes 919A and 919B. The initial natural remanent magnetization (NRM) of each undisturbed archive core section was measured using the WCC. Initial NRM intensities were typically 100 to >1000 mA/m. Generally, the initial NRM direction dips at 70° to 90° downward (i.e., is positive). Each core section was alternating-field (AF) demagnetized at 25 mT to remove low-coercivity (presumed to be secondary) components of magnetization. The 25-mT step reduced the intensities to typically 20% to 30% of the initial values, and inclinations typically were between 50° and 80° (positive or negative). The magnetostratigraphy of Site 919 (a composite section based on data from Holes 919A and 919B) is summarized in Figure 11. The interval 152-919A-1H, 0 cm, to 152-919A-6H-2, 35 cm (0-121 mbsf) is of dominantly normal polarity. Within this normal polarity magnetozone, two intervals comprise reversed and/or mixed polarity records (Intervals 152-919A-3H-5, 130 cm, to -6H, 80 cm, and 152-919A-3H-4, 120 cm, to -7H, 60 cm). Below 152-919B-6H-2, 35 cm (121 mbsf), the sediments are reversely magnetized. In Figure 12, we show a detailed plot of the 25-mT inclination directions between 117 and 123 mbsf. These data indicate that the magnetic directions downhole cant over from positive to negative inclinations across a 1.2-m interval near 120.5 mbsf, suggesting that the reversal marks a true geomagnetic field inversion and does not coincide with a stratigraphic break.

The presence of nannofossils (see "Biostratigraphy" section, this chapter) within the Site 919 sediments permits correlation of the magnetostratigraphic record with the geomagnetic polarity time scale. The junction between nannofossil Zones CN15 and CN14 (0.26 Ma) is positioned at about 56 mbsf (in Core 152-919A-7H). Consequently, the normal polarity sediments at the top of the (composite) section correlate with the Brunhes Chron. Assuming a constant sedimentation rate (21.5 cm/k.y.) above the CN15-14 junction, it is possible that the short reversed interval at about 25 mbsf (152-919A-3H-5, 130 cm, to -6H, 80 cm) corresponds to the Blake Event (at approximately 0.137 Ma). The CN14/CN13 boundary (i.e., the Pliocene/Pleistocene boundary) is positioned in Core 152-919B-6H (between 120 and 125 mbsf). This indicates that the reversal transition recorded in Section 152-919B-6H-2, between 0 and 80 cm, corresponds to the start of the Olduvai normal polarity event. This magnetobiostratigraphic correlation implies that reversely magnetized sediments, representing the upper part of the Matuyama Chron, are not present at Site 919. This implies that an unconformity, of about 1 m.y. duration, is positioned within the normal polarity magnetozone that juxtaposes the Brunhes and Olduvai chrons. However, no indication from the seismic records (see "Background and Scientific Objectives" section, this chapter) nor the sedimentological descriptions (see "Lithostratigraphy" section, this chapter) is seen for an unconformity being present at Site 919. The magnetobiostratigraphic data indicate a minimum sedimentation rate for the Pleistocene sediments of about 12.0 cm/k.y.

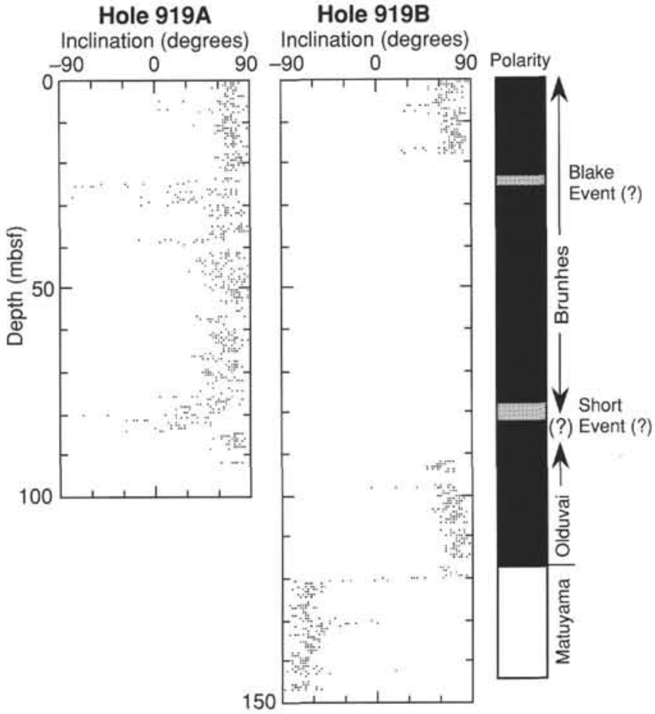

Figure 11. Summary of the magnetostratigraphy of Holes 919A and 919B, based on the directions obtained from the archive-half core sections after 25-mT demagnetization. Also shown are downhole plots of the inclination direction after 25-mT demagnetization. In the polarity column, black = normal, white = clearly reversed, shaded = possibly reversed and/or mixed.

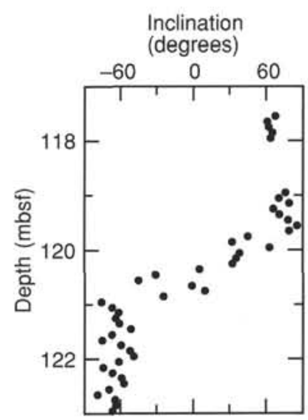

Figure 12. Detailed plot of inclination values from near Section 152-919B-6H-2, 35 cm (117–123 mbsf) showing the transitional (rather than abrupt) nature of the geomagnetic reversal at the start of the Olduvai Event.

SEDIMENTATION RATES

The shipboard nannofossil and planktonic foraminiferal biostratigraphies of Site 919 provide an age estimate of about 1.8 Ma for the sediments at a depth of about 128 mbsf. This suggests an average sedimentation rate of 7.1 cm/k.y. for the stratigraphic interval from 0 to 128 mbsf, assuming no significant unconformities in this interval. This sedimentation rate is in close agreement with that obtained at Site 918 (~8 cm/k.y.) for the same time interval. Other biostratigraphic horizons recorded on board the ship need to be confirmed and improved by shore-based studies before they can be used confidently as age control points. Unequivocal magnetic chron boundaries are not yet available for providing age control here.

ORGANIC GEOCHEMISTRY

The organic geochemistry analyses performed at Site 919 included measurements of elemental composition and volatile hydrocarbons (for methods see "Explanatory Notes" chapter, this volume).

Elemental Analyses

At Site 919, 72 sediment samples were analyzed for total carbon, inorganic carbon, total nitrogen, and total sulfur. Results are presented in Table 4 and Figures 13 to 15.

Table 4. Summary of organic chemistry analyses at Site 919.

Core, section, interval (cm)	Depth (mbsf)	TC (wt%)	IC (wt%)	TOC (wt%)	$CaCO_3$ (wt%)	TN (wt%)	TS (wt%)	TOC/TN (ratio)
152-919A-								
1H-1, 117–118	1.17	0.51		0.51	0.00	0.03	0.10	16.0
1H-2, 117–118	2.67	0.99	0.91	0.08	7.58	0.03	0.09	3.0
1H-3, 117–118	4.17	0.63	0.42	0.21	3.50	0.00	0.03	
1H-4, 117–118	5.67	0.39	0.10	0.29	0.83	0.03	0.09	10.8
1H-5, 117–118	7.17	0.57	0.36	0.21	3.00	0.03	0.11	6.4
2H-1, 30–31	8.30	0.34	0.18	0.16	1.50	0.03	0.00	5.3
2H-2, 40–41	9.90	0.66	0.54	0.12	4.50	0.00	0.07	
2H-3, 37–38	11.37	0.55	0.41	0.14	3.42	0.03	0.05	5.0
2H-4, 94–95	13.44	0.72	0.61	0.11	5.08	0.00	0.00	
2H-5, 55–56	14.55	0.82	0.64	0.18	5.33	0.03	0.06	6.9
2H-6, 29–30	15.79	1.41	1.28	0.13	10.66	0.09	0.00	1.4
3H-1, 37–38	17.87	1.47	1.53	0.00	12.74	0.00	0.00	
3H-2, 58–59	19.58	0.49	0.31	0.18	2.58	0.00	0.08	
3H-3, 15–16	20.65	0.48	0.20	0.28	1.67	0.02	0.00	11.8
3H-4, 26–27	22.26	0.66	0.27	0.39	2.25	0.02	0.10	15.7
3H-5, 73–74	24.23	0.70	0.48	0.22	4.00	0.02	0.09	9.0
3H-6, 23–24	25.23	0.45	0.28	0.17	2.33	0.00	0.26	
3H-7, 20–21	26.70	0.43	0.30	0.13	2.50	0.03	0.18	4.5
4H-1, 25–26	27.25	0.46	0.23	0.23	1.92	0.03	0.12	6.7
4H-2, 80–81	29.30	0.19	0.16	0.03	1.33	0.00	0.03	
4H-3, 88–89	30.88	0.40	0.33	0.07	2.75	0.00	0.00	
4H-4, 30–31	31.80	1.16	1.14	0.02	9.50	0.00	0.00	
4H-5, 37–38	33.37	0.33	0.12	0.21	1.00	0.03	0.00	6.2
4H-6, 55–56	35.05	0.24	0.22	0.02	1.83	0.00	0.00	
4H-7, 27–28	36.27	0.30	0.19	0.11	1.58	0.02	0.06	5.7
5H-1, 37–38	36.87	0.48	0.38	0.10	3.17	0.03	0.09	3.8
5H-2, 35–36	38.35	0.16	0.09	0.07	0.75	0.00	0.19	
5H-3, 25–26	39.75	0.92	0.86	0.06	7.16	0.00	0.00	
5H-4, 77–78	41.77	1.86	1.79	0.07	14.91	0.00	0.08	
5H-5, 32–33	42.82	0.19	0.12	0.07	1.00	0.00	0.07	
5H-6, 32–33	44.32	0.51	0.21	0.30	1.75	0.03	0.07	10.8
5H-7, 20–21	45.70	0.63	0.47	0.16	3.92	0.00	1.41	
6H-1, 93–94	46.93	0.72	0.53	0.19	4.41	0.00	0.82	
6H-2, 37–38	47.87	0.45	0.33	0.12	2.75	0.00	0.00	
6H-3, 78–79	49.78	0.49	0.36	0.13	3.00	0.00	0.00	
6H-4, 23–24	50.73	1.13	0.96	0.17	8.00	0.00	0.00	
6H-5, 69–70	52.69	1.03	0.95	0.08	7.91	0.04	0.13	2.1
6H-6, 61–62	54.11	0.34	0.15	0.19	1.25	0.05	0.11	4.2
6H-7, 15–16	55.15	0.54	0.35	0.19	2.92	0.00	0.06	
7H-2, 29–30	57.29	0.40	0.26	0.14	2.17	0.03	0.00	4.4
7H-4, 32–33	60.32	0.69	0.46	0.23	3.83	0.05	0.00	4.5
7H-6, 16–17	63.16	0.74	0.59	0.15	4.91	0.04	0.10	4.1
8H-1, 121–122	66.21	0.95	0.82	0.13	6.83	0.04	0.12	3.1
8H-3, 27–28	68.27	1.06	0.79	0.27	6.58	0.05	0.09	5.5
8H-5, 114–115	72.14	1.00	0.75	0.25	6.25	0.03	0.10	8.1
8H-7, 23–24	74.23	1.31	0.95	0.36	7.91	0.03	0.23	10.7
9H-2, 78–79	76.78	0.43	0.21	0.22	1.75	0.06	0.00	4.0
9H-4, 46–47	79.46	0.94	0.38	0.56	3.17	0.05	0.09	10.8
9H-6, 84–85	82.84	0.53	0.23	0.30	1.92	0.04	0.10	7.0
10H-1, 55–56	84.55	0.54	0.46	0.08	3.83	0.00	0.11	
10H-3, 68–69	87.68	0.71	0.50	0.21	4.17	0.04	0.06	5.4
10H-5, 61–62	90.61	0.25	0.13	0.12	1.08	0.05	0.00	2.6
152-919B-								
3H-2, 96–97	92.46	0.77	0.71	0.06	5.91	0.03	0.00	1.7
3H-4, 33–34	94.83	0.63	0.33	0.30	2.75	0.03	0.07	9.0
3H-6, 61–62	98.11	0.35	0.18	0.17	1.50	0.04	0.00	4.9
4H-1, 55–56	100.05	0.50	0.29	0.21	2.42	0.05	0.00	4.2
4H-3, 76–77	103.26	0.25	0.12	0.13	1.00	0.03	0.17	4.3
4H-5, 75–76	106.25	1.19	1.00	0.19	8.33	0.04	1.38	5.0
4H-7, 11–12	108.61	0.47	0.24	0.23	2.00	0.04	0.00	5.3
5H-2, 76–77	111.26	0.44	0.09	0.35	0.75	0.04	0.12	8.9
5H-4, 70–71	114.20	0.48	0.25	0.23	2.08	0.05	0.00	4.8
5H-6, 44–45	116.94	0.49	0.33	0.16	2.75	0.04	0.07	3.9
6H-2, 124–125	121.24	0.65	0.55	0.10	4.58	0.00	0.00	
6H-4, 109–110	124.09	0.35	0.21	0.14	1.75	0.05	0.00	3.0
6H-6, 48–49	126.48	2.39	2.21	0.18	18.41	0.04	0.03	4.5
7H-1, 73–74	128.73	0.27	0.21	0.06	1.75	0.04	0.00	1.5
7H-3, 117–118	132.17	0.34	0.12	0.22	1.00	0.04	0.00	5.2
7H-5, 50–51	134.50	0.34	0.13	0.21	1.08	0.05	0.06	4.6
7H-7, 36–37	137.36	0.55	0.22	0.33	1.83	0.05	0.10	6.9
8H-2, 39–40	139.39	0.45	0.30	0.15	2.50	0.04	0.07	3.4
8H-4, 27–28	142.27	0.38	0.25	0.13	2.08	0.03	0.06	4.5
8H-6, 27–28	145.27	0.14	0.09	0.05	0.75	0.04	0.00	1.2

Notes: TC = total carbon; IC = inorganic carbon; TOC = total organic carbon; $CaCO_3$ = calcium carbonate; TN = total nitrogen; TS = total sulfur; and TOC/TN = total organic carbon/total nitrogen rations.

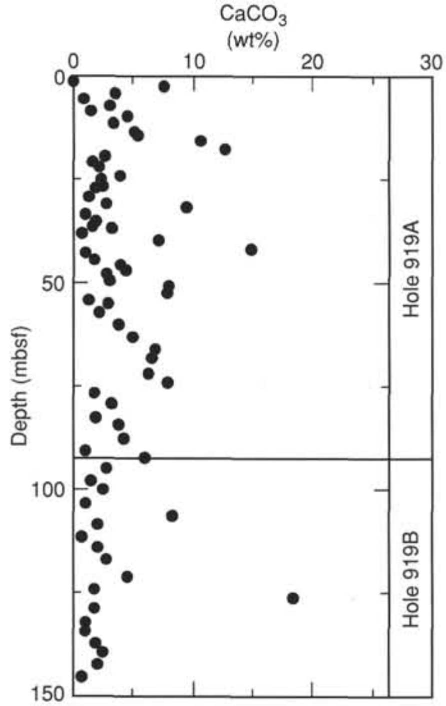

Figure 13. Results of calcium carbonate ($CaCO_3$) vs. depth in Holes 919A and 919B.

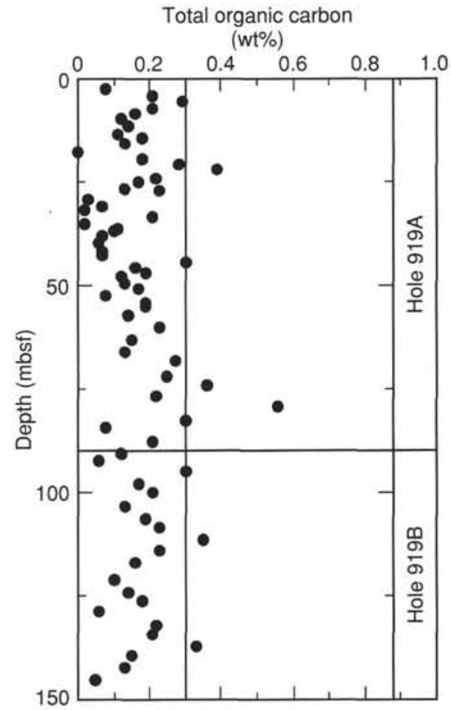

Figure 14. Results of TOC vs. depth in Holes 919A and 919B. Vertical line at 0.3 wt% indicates the TOC content of normal pelagic sediments (McIver, 1975).

Most sediments have calcium carbonate contents of less than 10 wt%; the highest value, of 18 wt%, occurs at 125 mbsf (Fig. 13). As reported in the "Lithostratigraphy" section (this chapter), carbonate is dominated by planktonic foraminifers. Total organic carbon (TOC) contents at Site 919 are low and range principally between about 0 and 0.4 wt% (Fig. 14). TOC spikes, Site 918, indicate that enhanced supplies of terrigenous organic matter could not be detected. The calcium carbonate and organic carbon records reflect the uniformity of the sediments recovered at Site 919, which comprise only one lithologic unit (see "Lithostratigraphy" section, this chapter). Total nitrogen concentrations at Site 919 are low and vary between 0 and 0.05 wt%. Total sulfur contents range from 0 to about 1.4 wt% (see Table 4). Sulfur occurs mainly as finely disseminated, authigenic pyrite within the claystones and siltstones (see "Lithostratigraphy" section, this chapter).

Composition of Organic Matter

TOC/total nitrogen values were used to estimate the amount of marine organic material. Most of these ratios are below 10, indicating that the main portion of the organic material is of marine origin (Fig. 15; Bordovskiy, 1965; Emerson and Hedges, 1988). However, in these organic carbon-lean sediments, TOC/TN values must be used cautiously (Mueller, 1977; see "Organic Geochemistry" section, "Site 915" chapter, this volume). Rock-Eval pyrolysis analyses were not performed at Site 919.

Volatile Hydrocarbons

Real-time monitoring of the volatile hydrocarbons methane (C_1), ethane (C_2), and propane (C_3) was performed in line with shipboard safety and pollution prevention considerations. One sample was taken from each core immediately after its arriving on deck and was measured using a Hach-Carle gas chromatograph. The results are presented in Table 5 and displayed in Figure 16. Methane concentrations are highest between about 150 and 85 mbsf (400 to 20,000 ppm), decreasing dramatically to near the detection limit of the gas chromatograph from 85 to 0 mbsf.

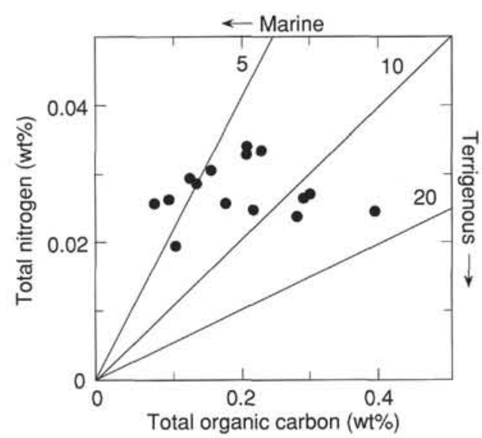

Figure 15. TOC vs. total nitrogen in sediments of Holes 919A and 919B. TOC/TN values of <10 suggest major proportions of marine organic matter; TOC/TN values >10 suggest major proportions of terrigenous organic matter.

The methane distribution shown in Figure 16 represents a pattern comparable to the uppermost part of the methane curve of Site 918. Unfortunately, the following decrease of methane with increasing depth could not be charted as a result of the termination of Hole 919B at 147 mbsf. The pore-water sulfate concentration is depleted at a depth of 85 mbsf, when methane starts to increase rapidly. This, as seen at Site 918, mirrors the effect of a steplike microbial decomposition of organic matter during sulfate reduction and the following methane generation (e.g., Claypool and Kvenvolden, 1983; Gieskes, 1983; see "Organic Geochemistry" section, "Site 918" chapter, this volume).

INORGANIC GEOCHEMISTRY

The interstitial water program at Site 919 concentrated on detailed sampling of the Pleistocene sediments for the following purposes:

Table 5. Results of headspace gas analysis using the Hach-Carle gas chromatograph, Site 919.

Core, section, interval (cm)	Depth (mbsf)	C_1 (ppm)	C_2 (ppm)	$C_{2=}$ (ppm)
152-919A-				
1H-5, 0–5	6.03	3		
2H-5, 0–5	14.03	5		
3H-5, 0–5	23.53	6		
4H-5, 0–5	33.03	8		
5H-5, 0–5	42.53	7		
6H-5, 0–5	52.03	5		
7H-5, 0–5	61.53	6		
8H-5, 0–5	71.03	59		
9H-5, 0–5	80.53	398		
10H-3, 0–5	87.03	795		
152-919B-				
1H-6, 0–5	7.53	3		
2H-5, 0–5	15.23	5		
3H-4, 0–5	94.53	1,347		
4H-4, 0–5	104.03	7,593		
5H-3, 0–5	112.03	10,850	1	1
6H-4, 0–5	123.03	14,023	1	1
7H-3, 140–145	132.43	21,779	1	
8H-5, 0–5	143.53	12,767	1	

Note: C_1 = methane, C_2 = ethane, and $C_{2=}$ = iso-ethane.

1. To delineate the possible signal of the seawater salinity increase during the last glaciation (McDuff, 1985; Schrag and DePaolo, 1993); and

2. To evaluate the sharpness of the boundary between the sulfate reduction and the methane production zones.

Both phenomena were investigated at Site 918 (see "Inorganic Geochemistry" section, "Site 918" chapter, this volume); at Site 919, emphasis has been placed on more detailed sampling and collecting samples for future isotope shore-based studies.

Methods are described in the "Explanatory Notes" chapter (this volume), and the data are presented in Table 6.

Biogenic Components

Data for alkalinity (HCO_3^-), sulfate, and ammonium are presented in Figure 17A. From a depth of about 20 to about 90 mbsf, the base of the sulfate reduction zone, the concentration-depth profiles are linear. This linearity suggests transport by diffusive exchange between about 20 and 90 mbsf, with sulfate reduction and associated processes of alkalinity and ammonium production occurring mainly at, or near, the boundary between the sulfate and methane zones. Clearly, the consumption of methane by sulfate-reducing bacteria prevents significant diffusive penetration of methane into the sulfate zone (see also "Organic Geochemistry" section, this chapter). Samples were collected for determining the carbon isotopic composition of dissolved carbon dioxide, which may shed light on the diffusion processes involved (Gamo et al., 1993).

Alkaline Earth Elements

As at Site 918, some small changes in dissolved calcium and magnesium are evident in the upper 20 mbsf, which can be traced to reactions within this zone. From about 20 mbsf to a depth of about 80 to 90 mbsf, the concentration-depth profiles are linear (Fig. 17A). Were this caused mainly by diffusive exchange, then a reaction zone must be located near the boundary between the sulfate and methane zones. A plot of the ratio of the calcium and magnesium concentrations (Mg/Ca) is presented in Figure 17B; it indicates a maximum at about 80 to 90 mbsf. High ratios of Mg/Ca and low sulfate concentrations are ideal conditions for dolomite formation (Baker and Kastner, 1981). Though little dolomite was detected in this zone (see "Lithostratigraphy" section, this chapter), further work on the solid phases will be required to detect any diagenetic alteration products. A plot of

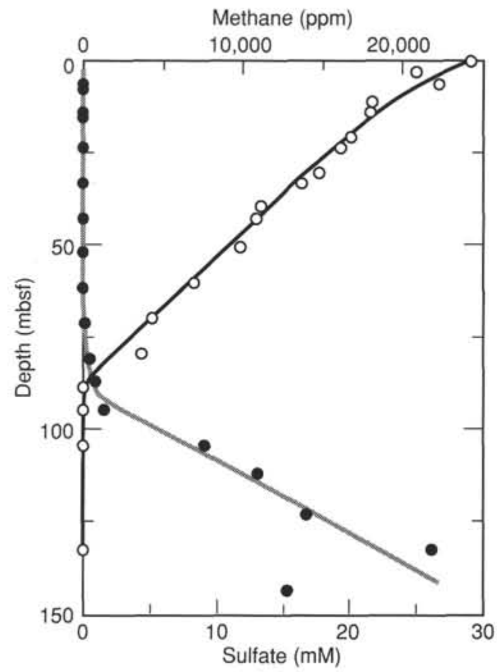

Figure 16. Results of methane measurements (solid circles) using the headspace technique vs. depth. Sulfate content of pore waters (open circles) from "Inorganic Geochemistry" section (this chapter).

the magnesium vs. calcium concentrations also reveals two linear correlations (Fig. 17C), again suggesting an important reaction zone at about 80 to 90 mbsf.

Dissolved strontium values indicate a rapid decrease with depth at this site (Fig. 17A). A similar decrease was observed at Site 918. More work on strontium isotopes will serve to evaluate the processes associated with the dissolving of strontium.

Alkali Metals

The data for alkali metal ions are presented in Figure 18A. Whereas dissolved lithium (as at Site 918) shows a rapid, logarithmic decrease with depth, dissolved potassium concentrations follow a linear decrease with depth, indicating diffusive transport to a location below the sampled section. Work on lithium isotopes may elucidate the nature of the processes that lead to the rapid decrease in dissolved lithium.

Dissolved sodium concentrations and Na/Cl values (Figs. 18A and 18B) show little change with depth. The accuracy of these data do not allow for detection of a potential maximum in the upper 50 mbsf.

Chloride

Dissolved chloride concentrations (Fig. 18B) indicate a well-developed maximum of about 572 mM at a depth of 50 mbsf. These data will be checked with more accurate methods in the shore-based laboratory, but changes of up to 1.8% in chloride concentrations are evident. As noted for Site 918, this maximum can be understood in terms of a remnant of higher salinity seawater present during the last glaciation (McDuff, 1985; Schrag and DePaolo, 1993). Further work on the distribution of the oxygen/hydrogen isotopic composition of the pore waters is planned.

Dissolved Silica

Data for dissolved silica are presented in Figure 18C. The concentrations are somewhat erratic and variable, presumably controlled by the local lithology. High reaction rates between silica and solid sili-

Table 6. Chemical composition of interstitial water composition at Site 919.

Core, section, interval (cm)	Depth (mbsf)	pH	Alkalinity (mM)	Salinity (g/kg)	SO_4^{2-} (mM)	NH_4^+ (mM)	Cl^- (mM)	H_4SiO_4 (µM)	Ca^{2+} (mM)	Mg^{2+} (mM)	Sr^{2+} (µM)	Li^+ (µM)	K^+ (mM)	Na^+ (mM)
Bottom water	0.00	8.1	2.35	34.97	29	0	558	50	10.54	54	87.00	29	10.4	480
152-919A-														
1H-2, 145–150	3.00	7.73	5.02		24.9	0.1	557	350	10.45	51.7	85.00	20	10.6	477
1H-4, 145 150	6.00	7.73	6.72		26.7	0.27	559	619	9.41	50	76.00	19	10	490
2H-2, 145–150	11.00		9.35	35	21.7	0.42	561	531	8.63	51.8	79.00	18	9.6	483
2H-4, 145–150	14.00			35	21.5	0.55	561	434	8.07	51.4	80.00	18	10	485
3H-2, 145–150	20.50	7.9	10.69	34.5	20.1	0.55	563	403	7.74	50.2	72.00	17	9.4	488
3H-4, 145–150	23.50	7.95	10.15	34.5	19.3	0.6	563	419	6.94	50.5	75.00	17	9.7	487
4H-2, 145–150	30.00	8	11.01	34.2	17.7	0.71	565	613	6.84	48.2	70.00	17	10.1	491
4H-4, 145–150	33.00			34.2	16.4	0.7	563	678	5.94	48.5	67.00	16	9.8	488
5H-2, 145–150	39.50	7.9	11.9	33.8	13.3	0.81	566	634	5.79	47.9	57.00	16	9.5	487
5H-4, 145–150	42.50	7.97	12.44	33.2	12.9	0.83	566	572	5.79	48.1	68.00	16	9.87	486
6H-3, 145–150	50.50	7.92	13.17	33.8	11.8	1	572	572	5.08	46.3	63.00	16	9.09	496
7H-3, 145–150	60.00	7.79	14.49	32	8.3	1.09	570	697	4.37	44.5	60.00	16	9.09	493
8H-3, 145–150	69.50	7.81	15.85	32.1	5.2	1.29	567	634	3.51	43.2	57.00	16	8.83	483
9H-3, 145–150	79.00	7.87	17.38	32.2	4.3	1.37	563	716	3.19	41.7	56.00	16	8.83	480
10H-3, 145–150	88.50	7.9	18.28	32.2	0	1.5	563	754	3.64	40.3	58.00	15	8.01	484
152-919B-														
3H-3, 145–150	94.50	7.95	19.52	32	0	1.57	564	663	3.79	39.5	60.00	15	8.21	487
4H-3, 145–150	104.00	7.85	18.75	32	0	1.68	560	703	4.09	39.2	60.00	15	8.15	482
7H-3, 145–150	132.50	7.75	18.85	32.5	0	1.72	558	744	4.84	38.2	65.00	16	7.57	481

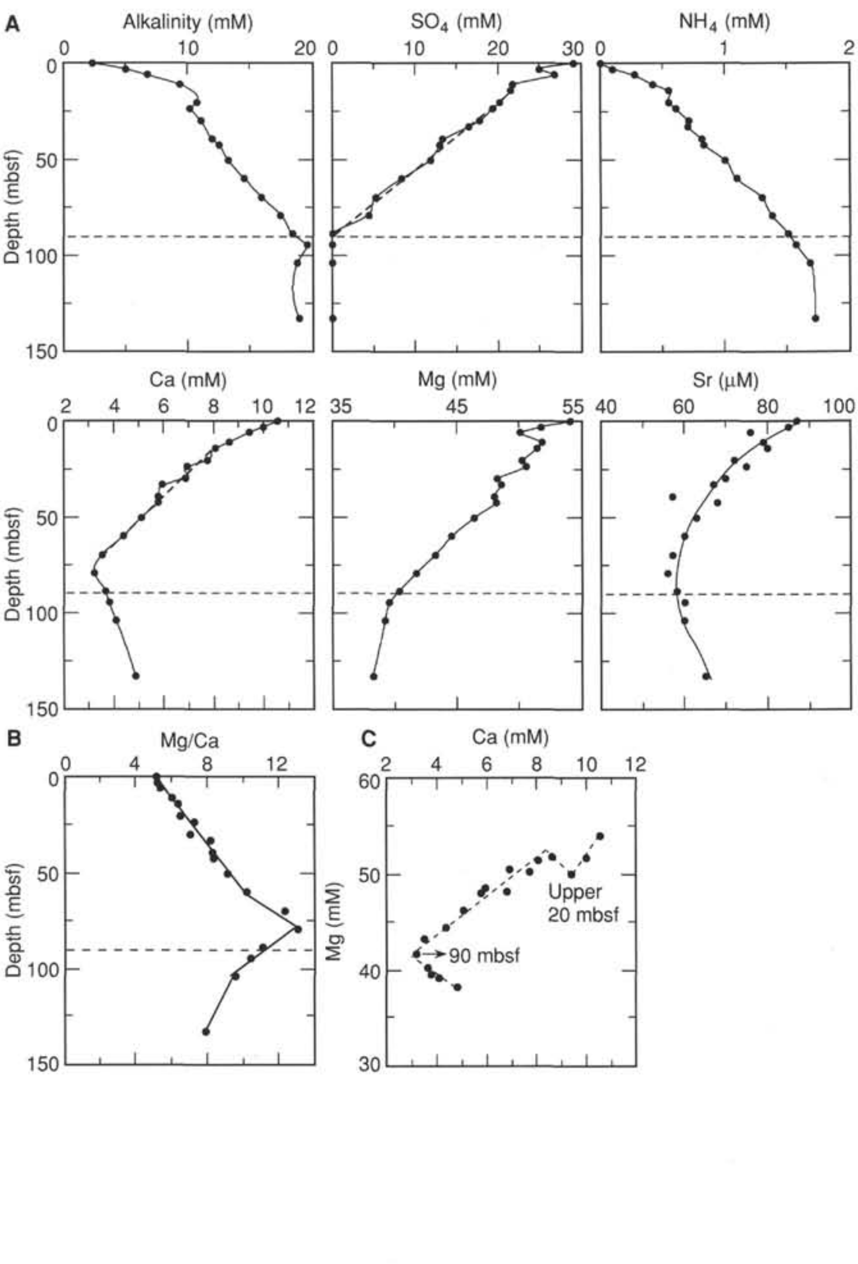

Figure 17. **A.** Distribution of biogenic elements (alkalinity, SO_4, NH_4), alkaline earth elements (Ca, Mg, Sr) in interstitial waters at Site 919. **B.** Mg/Ca values for Site 919. **C.** Correlation of Ca vs. Mg, Site 919. Horizontal dashed lines delineate the sulfate/methane boundary.

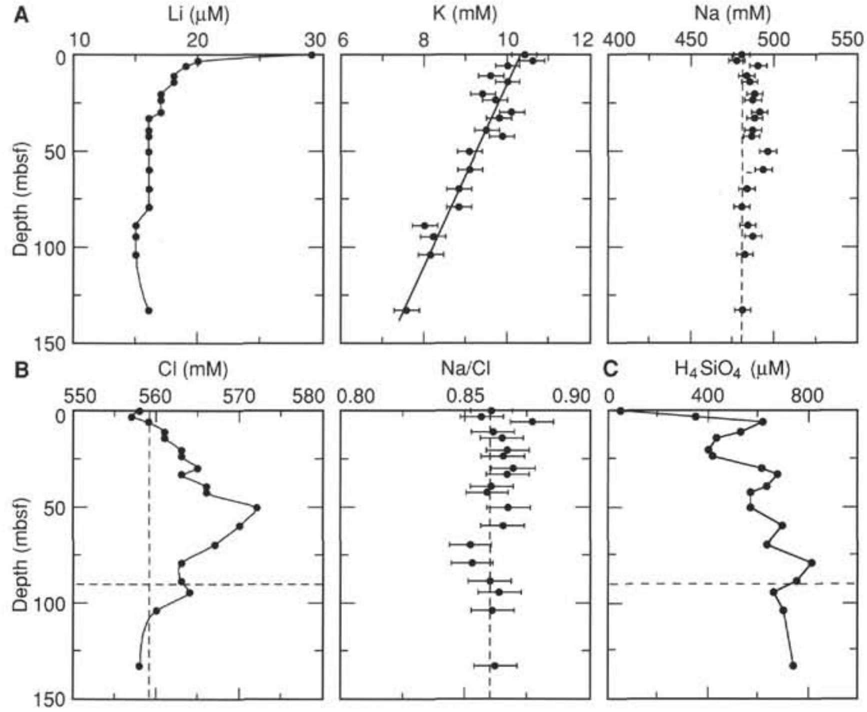

Figure 18. **A.** Distribution of alkali metals (Li, K, Na) in interstitial waters at Site 919. **B.** Dissolved chloride and Na/Cl values for Site 919. **C.** Dissolved silica, Site 919. Horizontal dashed lines delineate the sulfate/methane boundary. Vertical dashed lines indicate present-day values for seawater.

cate phases have often been invoked for understanding this variability in dissolved concentrations (e.g., Gieskes et al., 1993).

Summary and Conclusions

Although detailed shore-based isotope work will be necessary to support the interpretations of the concentration changes observed in the interstitial waters of Site 919, various important conclusions can be reached at this stage:

1. A transient signal of increased chloride concentrations supports the salinity increases associated with the last glacial period. The chloride maximum is located at about 50 mbsf.
2. Much of the sulfate depletion observed in the upper 90 m of the sediment column was caused by bacterial sulfate reduction, presumably involving the oxidation of dissolved methane as it diffused across the sulfate/methane boundary at about 90 mbsf.
3. Processes involving the consumption of dissolved calcium and magnesium appear to be concentrated between about 80 and 90 mbsf. Perhaps these removal processes involved reactions associated with both the alteration of volcanic matter and the formation of dolomite.

PHYSICAL PROPERTIES

Introduction

APC-coring was successful at Site 919. The quality of the cores and the continuous recovery permitted us to analyze in detail the physical properties of the Pleistocene and upper Pliocene sediments in this part of the western Irminger Basin. Hole 919A was APC-cored to a depth of 93.5 mbsf. Hole 919B was APC-cored from 0 to 18.7 mbsf, then washed to a depth of 93.5 mbsf, and APC-cored to a depth of 147.0 mbsf. Only multisensor track (MST) data were obtained from the two uppermost cores in Hole 919B, and no physical properties were measured as this material was reserved for tephra and isotope sampling (this interval was measured in Hole 919A).

Multisensor Track (MST)

All cores recovered at Site 919 were processed through the MST, with the exception of cores in double liners (because of liner damage). In these instances, the core diameter was too great for their passage through the magnetic susceptibility (Bartington) loop.

Sediments recovered at Site 919 were assigned to mechanical Unit M1, which correlates with lithologic Unit I (see "Lithostratigraphy" section, this chapter). Mechanical Unit M1 is characterized by natural gamma of 480 to 1050 TC, magnetic susceptibility of 200 to 1200 cgs, *P*-wave velocity of 1475 to 1575 m/s, and GRAPE wet bulk density of 1.4 to 2.1 g/cm^3 (Fig. 19).

On the basis of *P*-wave velocity and GRAPE bulk density variations, mechanical Unit M1 can be divided into three subunits: M1a, M1b, and M1c. Mechanical Subunit M1a constitutes the upper 64 m of the succession. The upper 40 m of this subunit exhibits an increase downcore in GRAPE bulk density and a reduction in porosity. This is common in marine sediments and is associated with compactive dewatering. Over the same interval, magnetic susceptibility increases downcore from 400 to 850 cgs. *P*-wave velocity averages 1500 ± 25 m/s and fluctuates throughout Subunit M1a.

Subunit M1b is about 10 m thick (Cores 152-919A-7H to -8H; 64–74 mbsf). It is defined primarily by a sharp increase in *P*-wave velocity (to about 1540 m/s at 65 mbsf). The *P*-wave velocity continues to increase with depth throughout Subunit M1b to a maximum of ≈1575 m/s. The MST data for Subunit M1B are significantly different in character from the sediments above and below: GRAPE bulk density and magnetic susceptibility signals are more homogeneous than for Subunits M1a and M1c.

Subunit M1c, from 74 to 150 mbsf (Cores 152-919A-9H to -10H and 152-919B-3H to -8H), is characterized by greater variability in the MST signal. This suggests a more heterogeneous sediment assemblage than that of Subunit M1b. The MST record for Subunits M1a and M1c is similar. *P*-wave velocities in Subunit M1c are consistently higher than those in Subunit M1a, with velocities averaging 1525 m/s (compared to 1500 m/s for Subunit M1a).

The MST signal is characterized by many smaller-scale changes that belie the complexity of the sediment packages referred to in the Site 919 "Lithostratigraphy" section (this chapter). Turbiditic sequences and fining-upward units are revealed in great detail on a section-by-section scale, particularly in terms of the magnetic susceptibility and natural gamma signals. A frequent association is found between fine-grained units, low magnetic susceptibility, and locally

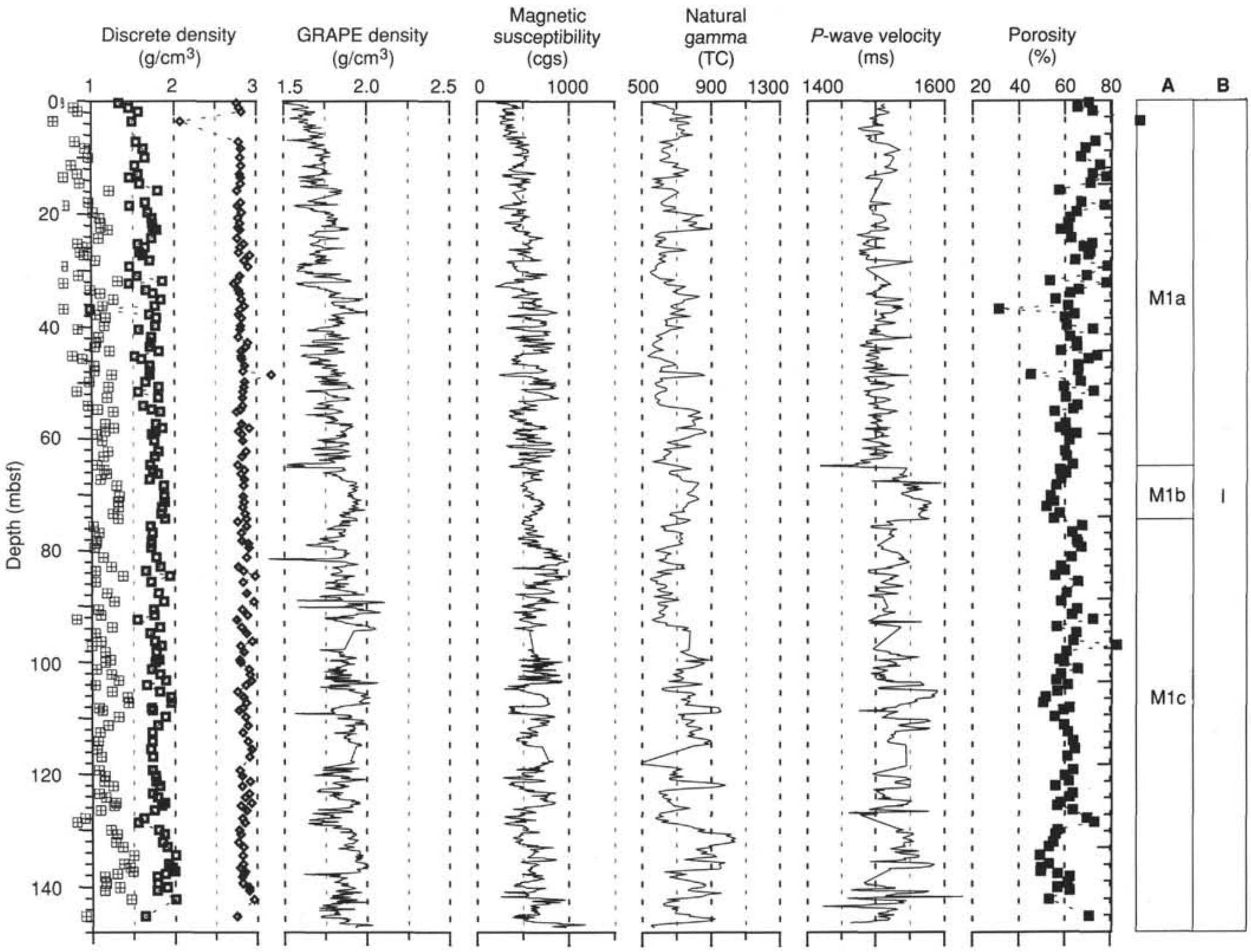

Figure 19. Composite plot of MST and discrete index-property data for sediments recovered at Site 919. MST data comprise GRAPE wet bulk density, magnetic susceptibility, *P*-wave velocity, and natural gamma. Discrete measurements include wet bulk density (open squares), grain density (open diamonds), dry density (hatched squares), and porosity (filled squares). **A** = mechanical units, **B** = lithologic unit.

high natural gamma (e.g., Section 152-919A-3H-4). Several tephra layers are identified in the sediment column of Site 919 (see "Lithostratigraphy" section, this chapter). Note that only the more acidic tephra layers are apparent from the MST magnetic susceptibility record (Fig. 20). The acidic tephra layers produce a magnetic susceptibility minimum, while the basaltic tephra layers show no deviation from the background sediments. This suggests that basaltic tephra and sediments contain a similar amount of magnetically susceptible minerals, while the acidic tephra contain reduced amounts of magnetically susceptible minerals.

On a whole-core scale, some cyclicity in the MST signatures may be present. However, it is not possible, on the basis of shipboard work alone, to demonstrate such cyclicity or to infer the response of the sediments to glacial-interglacial forcing.

The MST data from Site 919 cannot be used to support the existence of a major unconformity within the Pliocene–Pleistocene, as is suggested by the biostratigraphic data from Site 919 (see "Biostratigraphy" section, this chapter). As the MST data have appeared particularly useful for distinguishing variations in sediment provenance within and between lithologic units (for example, see "Physical Properties" sections, "Site 915" and "Site 916" chapters, this volume), we conclude that no provenance shift occurred during the time period represented by this hypothetical erosional or nondepositional surfaces.

Index Properties

Wet-bulk density, grain density, dry density, water content, porosity. and void ratio (see "Physical Properties" section, "Explanatory Notes" chapter, this volume) were determined for 134 discrete samples. These data are tabulated in Table 7 and illustrated in Figure 19.

Mechanical Subunit M1a is delineated by a general downcore reduction in porosity, from ≈70% at the seabed, to ≈50% at the M1a/M2a boundary (65 mbsf). This decrease also is associated with a lessening in the scatter of the data. Grain density remains constant (≈2.8 g/cm^3) throughout Subunit M1a. A gradual increase in discrete wet bulk density parallels the increase in GRAPE wet bulk density.

The index-properties data for mechanical Subunit M1b are remarkably consistent. A reduction in porosity (to a low of ≈50%) and a corresponding increase in bulk density (to ≈1.9 g/cm^3) separate this subunit from Subunits M1a and M1c. There is no change in grain density (2.8 g/cm^3) from the adjacent subunits.

The boundary between Subunits M1b and M1c is most easily seen as shifts in the index-property data. Porosity jumps from about 50% at the base of Subunit M1b (74 mbsf; Section 152-919A-8H-CC) to 70% at the top of Subunit M1c and thereafter shows a gradual reduction downcore to <50% at 140 mbsf (152-919B-8H-2, 100 cm). The jump in porosity between Subunits M1b and M1c correlates well with the

Table 7. Index property data for Site 919.

Core, section, interval (cm)	Depth (mbsf)	Water content W_t (%)	Bulk density (g/cm³) MB	Grain density (g/cm³) MC	Dry Density (g/cm³) MB	Porosity (%) MC	Void ratio MC
152-919A-							
1H-1, 30–32	0.30	118.3	1.33	2.77	0.61	70.3	3.20
1H-1, 118–120	1.18	86.0	1.45	2.79	0.78	65.5	2.34
1H-2, 30–32	1.80	88.8	1.57	2.82	0.83	72.0	2.44
1H-3, 59–61	3.59	177.0	1.49	2.08	0.54	92.8	3.59
1H-5, 120–122	7.20	94.7	1.54	2.78	0.79	73.2	2.57
2H-1, 31–33	8.31	76.8	1.62	2.82	0.92	68.9	2.11
2H-2, 45–47	9.95	71.4	1.65	2.81	0.96	67.1	1.96
2H-3, 38–40	11.38	102.5	1.53	2.82	0.75	75.6	2.82
2H-4, 37–39	12.87	89.5	1.57	2.80	0.83	72.2	2.45
2H-4, 96–98	13.46	121.9	1.46	2.82	0.66	78.2	3.35
2H-5, 57–59	14.57	85.2	1.59	2.82	0.86	71.2	2.34
2H-6, 31–33	15.81	48.7	1.80	2.77	1.21	57.6	1.32
3H-1, 34–36	17.84	71.3	1.65	2.81	0.96	67.2	1.96
3H-1, 100–102	18.50	118.5	1.46	2.78	0.67	77.2	3.21
3H-2, 60–62	19.60	65.8	1.68	2.82	1.01	65.2	1.81
3H-3, 16–18	20.66	58.2	1.73	2.78	1.09	62.2	1.58
3H-3, 105–107	21.55	56.8	1.74	2.81	1.11	61.4	1.56
3H-4, 27–29	22.27	56.6	1.74	2.78	1.11	61.5	1.54
3H-4, 68–70	22.68	49.9	1.79	2.80	1.19	58.2	1.36
3H-5, 74–76	24.24	59.1	1.73	2.77	1.08	62.6	1.60
3H-6, 24–26	25.24	89.0	1.56	2.85	0.83	71.8	2.48
3H-6, 80–82	25.80	73.7	1.65	2.80	0.95	68.3	2.02
3H-7, 18–20	26.68	85.1	1.58	2.78	0.85	70.9	2.31
4H-1, 21–23	27.21	79.8	1.62	2.92	0.90	70.2	2.28
4H-1, 112–114	28.12	63.5	1.70	2.86	1.04	64.6	1.77
4H-2, 77–79	29.27	123.9	1.46	2.91	0.65	78.8	3.52
4H-3, 90–92	30.90	85.1	1.55	2.80	0.84	69.7	2.33
4H-4, 32–34	31.82	41.9	1.86	2.77	1.31	53.6	1.13
4H-4, 74–76	32.24	121.6	1.46	2.73	0.66	78.0	3.24
4H-5, 40–42	33.40	69.1	1.66	2.79	0.98	66.2	1.88
4H-5, 100–102	34.00	57.9	1.74	2.81	1.10	62.4	1.59
4H-6, 57–59	35.07	45.3	1.84	2.82	1.26	55.9	1.25
4H-7, 29–31	36.29	55.6	1.76	2.85	1.13	61.5	1.55
5H-1, 34–36	36.84	48.8	0.98	2.80	0.66	31.4	1.34
5H-1, 123–125	37.73	63.2	1.70	2.78	1.04	64.2	1.72
5H-2, 32–34	38.32	52.6	1.78	2.82	1.17	59.9	1.45
5H-3, 22–24	39.72	54.2	1.77	2.81	1.15	60.7	1.48
5H-3, 95–97	40.45	89.2	1.57	2.80	0.83	72.3	2.44
5H-4, 74–76	41.74	59.1	1.72	2.78	1.08	62.3	1.60
5H-5, 29–31	42.79	63.5	1.72	2.89	1.05	65.1	1.80
5H-5, 101–103	43.51	64.7	1.70	2.87	1.03	65.2	1.81
5H-6, 28–30	44.28	49.1	1.81	2.82	1.21	58.2	1.35
5H-6, 116–118	45.16	99.7	1.52	2.82	0.76	74.1	2.74
5H-7, 17–19	45.67	81.0	1.60	2.82	0.89	70.1	2.23
6H-1, 90–92	46.90	65.8	1.69	2.85	1.02	65.7	1.83
6H-2, 34–36	47.84	65.2	1.70	2.84	1.03	65.7	1.81
6H-2, 101–103	48.51	37.4	1.70	3.18	1.24	45.2	1.16
6H-3, 75–77	49.75	70.7	1.65	2.86	0.97	66.8	1.97
6H-4, 19–21	50.69	50.8	1.81	2.85	1.20	59.6	1.41
6H-4, 99–101	51.49	90.9	1.56	2.84	0.82	72.6	2.52
6H-5, 66–68	52.66	52.4	1.80	2.83	1.18	60.5	1.45
6H-6, 58–60	54.08	70.6	1.62	2.83	0.95	65.6	1.95
6H-6, 120–122	54.70	60.9	1.72	2.81	1.07	63.7	1.67
6H-7, 12–14	55.12	45.3	1.83	2.76	1.26	55.6	1.22
7H-2, 26–28	57.26	53.2	1.77	2.82	1.16	60.2	1.47
7H-2, 106–108	58.06	46.8	1.86	2.91	1.26	57.8	1.33
7H-3, 13–15	58.63	53.5	1.77	2.78	1.16	60.4	1.45
7H-3, 68–70	59.18	62.7	1.73	2.82	1.06	64.9	1.72
7H-4, 29–31	60.29	56.5	1.75	2.83	1.12	61.9	1.56
7H-5, 71–73	62.21	51.8	1.80	2.87	1.19	60.1	1.45
7H-6, 13–15	63.13	54.7	1.76	2.82	1.14	60.7	1.51
7H-7, 16–18	64.66	61.4	1.71	2.77	1.06	63.4	1.66
8H-1, 58–60	65.58	51.8	1.73	2.85	1.14	57.8	1.44
8H-1, 125-127	66.25	52.8	1.79	2.81	1.17	60.5	1.45
8H-2, 77-79	67.27	54.3	1.70	2.85	1.10	58.3	1.51
8H-3, 30-32	68.30	44.5	1.87	2.84	1.30	56.4	1.24
8H-4, 75-77	70.25	41.5	1.88	2.83	1.33	53.9	1.15
8H-5, 23-25	71.23	43.1	1.88	2.85	1.32	55.4	1.20
8H-5, 115-117	72.15	40.5	1.85	2.83	1.32	52.1	1.12
8H-6, 84-86	73.34	47.2	1.84	2.86	1.25	57.7	1.32
8H-7, 25-27	74.25	43.2	1.88	2.88	1.31	55.4	1.21
9H-1, 25-27	74.75	59.9	4.18	2.77	2.62	153.1	1.62
9H-1, 111-113	75.61	68.0	1.71	2.88	1.02	67.4	1.91
9H-2, 80-82	76.80	59.9	1.73	2.81	1.08	63.3	1.65
9H-3, 66-68	78.16	63.6	1.72	2.82	1.05	65.3	1.75
9H-3, 125-127	78.75	64.2	1.72	2.90	1.05	65.8	1.82
9H-4, 48-50	79.48	67.0	1.72	2.91	1.03	67.2	1.90
9H-5, 68-70	81.18	56.7	1.78	2.88	1.14	62.8	1.59
9H-6, 87-89	82.87	48.6	1.83	2.78	1.23	58.3	1.32
9H-7, 15-17	83.65	59.2	1.65	2.83	1.04	60.0	1.64
10H-1, 52-54	84.52	41.6	1.94	2.98	1.37	55.7	1.21
10H-2, 10-12	85.60	64.9	1.71	2.83	1.04	65.8	1.80
10H-3, 65-67	87.65	53.0	1.80	2.87	1.18	60.9	1.49
10H-4, 64-66	89.14	47.3	1.87	2.97	1.27	58.6	1.37
10H-5, 59-61	90.59	62.3	1.75	2.82	1.08	65.4	1.72
10H-6, 11-13	91.61	58.5	1.75	2.89	1.11	63.2	1.65
152-919B-							
3H-2, 92–94	92.42	91.3	1.55	2.76	0.81	72.3	2.46
3H-3, 71–73	93.71	46.7	1.82	2.81	1.24	56.6	1.28
3H-4, 30–32	94.80	64.5	1.70	2.88	1.04	65.2	1.81
3H-5, 29–31	96.29	59.2	1.76	2.95	1.11	64.0	1.70
3H-5, 112–114	97.12	85.3	1.84	2.80	0.99	82.8	2.34
3H-6, 64–66	98.14	53.9	1.78	2.85	1.16	60.8	1.50
3H-7, 57–59	99.57	48.6	1.81	2.79	1.22	57.8	1.33
4H-1, 51–53	100.01	52.8	1.76	2.80	1.15	59.5	1.45
4H-2, 24–26	101.24	64.2	1.72	2.91	1.05	65.7	1.82
4H-2, 120–122	102.20	48.7	1.82	2.92	1.23	58.3	1.39
4H-3, 72–74	103.22	44.0	1.89	2.93	1.31	56.4	1.26
4H-4, 11–13	104.11	60.8	1.66	2.87	1.03	61.3	1.70
4H-4, 123–125	105.23	47.1	1.82	2.77	1.23	56.8	1.27
4H-5, 78–80	106.28	37.3	1.95	2.84	1.42	51.7	1.03
4H-6, 32–34	107.32	36.1	1.96	2.87	1.44	50.7	1.01
4H-6, 118–120	108.18	58.8	1.72	2.83	1.08	62.1	1.63
4H-7, 15–17	108.65	54.5	1.73	2.79	1.12	59.6	1.48
5H-1, 75–77	109.75	43.3	1.89	2.87	1.32	55.8	1.21
5H-2, 79–81	111.29	51.6	1.80	2.90	1.19	59.8	1.46
5H-3, 55–57	112.55	57.6	1.72	2.83	1.09	61.6	1.59
5H-4, 65–67	114.15	60.8	1.72	2.89	1.07	63.6	1.72
5H-5, 53–55	115.53	62.7	1.71	2.94	1.05	64.4	1.80
5H-6, 39–41	116.89	56.8	1.73	2.91	1.10	61.2	1.61
6H-1, 84–86	119.34	60.7	1.73	2.79	1.07	63.7	1.65
6H-2, 29–31	120.29	53.7	1.76	2.82	1.15	60.2	1.48
6H-2, 126–128	121.26	55.6	1.77	2.92	1.14	61.8	1.58
6H-3, 63–65	122.13	45.9	1.82	2.82	1.25	55.9	1.27
6H-4, 50–52	123.50	60.3	1.73	2.91	1.08	63.4	1.71
6H-4, 112–114	124.12	55.0	1.79	2.85	1.15	62.1	1.53
6H-5, 65–67	125.15	46.6	1.87	2.93	1.28	58.1	1.33
6H-5, 117–119	125.67	46.3	1.84	2.80	1.26	56.9	1.27
6H-6, 45–47	126.45	59.3	1.75	2.87	1.10	63.4	1.66
6H-7, 44–46	127.94	78.5	1.62	2.83	0.91	69.7	2.16
7H-1, 70–72	128.70	92.3	1.56	2.86	0.81	72.9	2.57
7H-2, 50–52	130.00	47.8	1.81	2.79	1.22	57.1	1.30
7H-2, 121–123	130.71	44.5	1.87	2.80	1.29	56.2	1.22
7H-3, 119–121	132.19	44.1	1.85	2.78	1.28	55.2	1.20
7H-4, 51–53	133.01	40.1	1.91	2.84	1.36	53.4	1.11
7H-5, 52–54	134.52	33.8	2.01	2.82	1.50	49.5	0.93
7H-6, 52–54	136.02	39.7	1.92	2.83	1.38	53.4	1.10
7H-6, 117–119	136.67	35.2	1.97	2.80	1.45	50.0	0.96
7H-7, 37–39	137.37	34.2	1.99	2.85	1.49	49.6	0.95
8H-1, 24–26	137.74	45.1	1.88	2.84	1.30	57.1	1.25
8H-1, 79–81	138.29	55.9	1.78	2.82	1.14	62.3	1.54
8H-2, 36–38	139.36	54.3	1.79	2.83	1.16	61.5	1.50
8H-2, 112–114	140.12	44.0	1.91	2.90	1.33	57.0	1.25
8H-3, 10–12	140.60	55.6	1.78	2.90	1.15	62.2	1.58
8H-4, 23–25	142.23	37.3	2.01	2.96	1.46	53.3	1.08
8H-6, 24–26	145.24	78.9	1.64	2.75	0.91	70.5	2.12

Note: Data were calculated according to Method B (MB) or Method C (MC) as defined in "Physical Properties" section, "Explanatory Notes" chapter (this volume).

decrease in *P*-wave velocity (MST) at the same boundary. Although grain density in Subunit M1c generally is similar to values found in the overlying sediments, the variability is significantly greater.

Velocimetry

P-wave velocity was measured on cores recovered from Holes 919A and 919B using the digital sonic velocimeter (DSV) (Table 8). Measurements were performed at an average interval of approximately 1 m. Velocities were measured both parallel (V_z) and perpendicular (V_x) to the core axis, as outlined in the "Explanatory Notes" chapter ("Physical Properties" section, this volume). Considerable attenuation of the acoustic signal, particularly in the longitudinal direction, often hampered the exact determination of velocities. Small cracks that formed during insertion of the transducers into the sediment undoubtedly contributed to this phenomenon. In the lower part of Hole 919B, between 118.5 and 147.0 mbsf (Cores 152-919B-6H to -8H), the attenuation was so strong that no longitudinal velocities could be obtained.

Table 8. *P*-wave velocity measurements for Holes 919A and 919B.

Core, section, interval (cm)	Depth (mbsf)	Calculated velocity V_z (m/s)	Calculated velocity V_x (m/s)
152-919A-			
1H-1, 36	0.36	1487	1538
1H-1, 115	1.15	1467	1435
1H-2, 29	1.79	1481	1473
1H-3, 23	3.23	1467	1538
1H-4, 123	5.73	1484	1544
1H-5, 126	7.26	1485	1571
2H-1, 35	8.35	1462	1446
2H-2, 42	9.92	1493	1459
2H-2, 33	9.83	1487	1529
2H-4, 34	12.84	1495	1640
2H-4, 97	13.47	1447	1642
2H-5, 61	14.61	1506	1606
3H-1, 32	17.82	1489	1574
3H-1, 97	18.47	1408	1262
3H-2, 64	19.64	1501	1613
3H-3, 14	20.64	1503	1590
3H-3, 102	21.52	1486	1581
3H-4, 32	22.32	1506	1636
3H-4, 71	22.71	1508	1656
3H-5, 71	24.21	1528	1560
3H-6, 24	25.24	1483	1311
3H-6, 81	25.81	1492	
3H-7, 19	26.69	1477	1581
4H-1, 19	27.19	1483	1578
4H-1, 109	28.09	1518	1597
4H-2, 78	29.28	1391	1102
4H-3, 88	30.88	1481	1535
4H-4, 36	31.86	1604	1298
4H-4, 73	32.23		1613
4H-5, 38	33.38	1427	1593
4H-5, 97	33.97	1505	1476
4H-6, 64	35.14	1539	1506
4H-7, 30	36.3	1524	1514
5H-1, 31	36.81	1553	1618
5H-1, 119	37.69	1500	1673
5H-2, 30	38.3	1532	1428
5H-3, 19	39.69	1514	1709
5H-3, 42	39.92		1701
5H-4, 71	41.71	1551	1616
5H-5, 26	42.76	1497	1656
5H-5, 98	43.48	1498	1642
5H-6, 26	44.26	1337	1523
5H-6, 121	45.21	1395	1626
5H-7, 19	45.69	1478	1626
6H-1, 91	46.91	1481	1523
6H-2, 32	47.82	1492	1484
6H-2, 106	48.56	1492	1677
6H-3, 80	49.8	1483	1653
6H-4, 16	50.66	1531	1709
6H-4, 96	51.46	1461	1444
6H-5, 71	52.71	1514	1691
6H-6, 62	54.12	1513	1793
6H-6, 118	54.68	1523	1724
6H-7, 12	55.12	1558	1666
7H-2, 29	57.29	1546	1684
7H-2, 102	58.02	1416	1547
7H-3, 65	59.15	1498	1680
7H-4, 34	60.34	1510	1677
7H-4, 88	60.88	1528	1653
7H-5, 69	62.19	1486	1709
7H-6, 16	63.16	1418	1713
7H-7, 14	64.64	1540	1746
8H-1, 55	65.55	1532	1514
8H-1, 126	66.26	1513	1663
8H-2, 75	67.25	1506	1622
8H-3, 30	68.3	1544	1649
8H-4, 75	70.25	1541	1684
8H-5, 25	71.25	1548	1666
8H-5, 116	72.16	1566	1512
8H-6, 84	73.34	1542	1743
8H-7, 25	74.25	1554	1712
9H-1, 25	74.75	1512	1596
9H-1, 112	75.62	1503	1574
9H-2, 81	76.81	1507	1709
9H-3, 67	78.17	1400	1727
9H-3, 125	78.75	1501	1742
9H-4, 48	79.48	1482	1723
9H-5, 69	81.19	1449	1746
9H-6, 88	82.88		1765
9H-7, 16	83.66	1482	1716
10H-1, 54	84.54	1504	1720
10H-2, 10	85.6	1506	1822
10H-3, 66	87.66	1524	1747
10H-4, 74	89.24	1495	1946
10H-4, 85	89.35		1622
10H-5, 60	90.6	1426	1556
10H-6, 12	91.62	1547	1793
152-919B-			
3H-2, 11	91.61	1293	1639
3H-2, 89	92.39	1509	1532
3H-3, 69	93.69	1545	1801
3H-5, 27	96.27	1562	1839
3H-5, 110	97.1	1521	1789
3H-6, 62	98.12	1569	1860
3H-7, 55	99.55	1553	1797
4H-1, 49	99.99	1524	1770
4H-2, 25	101.25	1458	1691
4H-2, 118	102.18	1529	1659
4H-3, 70	103.2	1514	1754
4H-4, 18	104.18		1758
4H-4, 127	105.27	1236	1541
4H-5, 82	106.32	1496	1864
4H-6, 36	107.36	1162	1847
4H-6, 116	108.16	1508	1814
4H-7, 20	108.7		1731
5H-1, 79	109.79	1063	1568
5H-2, 82	111.32	1547	1785
5H-3, 59	112.59	1035	1762
5H-4, 88	114.38	1500	1822
5H-5, 59	115.59	1550	1754
5H-6, 44	116.94	1341	1774
6H-1, 80	119.3		1636
6H-2, 32	120.32		1735
6H-2, 122	121.22		1512
6H-3, 59	122.09	1556	1743
6H-4, 48	123.48		1747
6H-4, 109	124.09	1254	1670
6H-5, 70	125.2		1758
6H-5, 121	125.71		1847
6H-6, 50	126.5		1762
6H-7, 41	127.91		1429
7H-1, 67	128.67		1694
7H-2, 52	130.02		1774
7H-2, 118	130.68	1566	1814
7H-3, 19	131.19		1835
7H-3, 116	132.16	1575	1785
7H-4, 49	132.99		1801
7H-5, 49	134.49		1609
7H-6, 47	135.97		1810
7H-6, 113	136.63		1659
7H-7, 35	137.35		1762
8H-1, 78	138.28		1529
8H-2, 34	139.34		1758
8H-2, 112	140.12		1673
8H-3, 12	140.62		1629

Note: Data were calculated according to Method B or Method C, as defined in "Physical Properties" section, "Explanatory Notes" chapter (this volume).

In Hole 919A (Cores 152-919A-2H to -3H; 8.0–27.0 mbsf) and in Hole 919B (Cores 152-919B-3H to -6H; 90.0–128.0 mbsf), a number of the measured velocities were less than 1400 m/s. These slow velocities probably were the result of the inability of the DSV to recognize and measure properly the arrival time for strongly attenuated signals.

The longitudinal velocities (V_z) show a slight increase from ≈1475 m/s at the seafloor to about ≈1550 m/s at 140 mbsf (Fig. 21). The transverse velocities (V_x) are consistently higher than the longitudinal velocities (V_z) (about 1550 m/s at the seafloor, increasing to about 1800 m/s at 90–100 mbsf and at deeper levels). Note the increase in the difference (acoustic anisotropy) between the two velocities with increasing depth. This difference increases steadily from about 50 m/s at the seafloor to about 200 m/s at 100 mbsf. Below 100 mbsf, this difference tends to be constant at 200 to 250 m/s (Fig. 21).

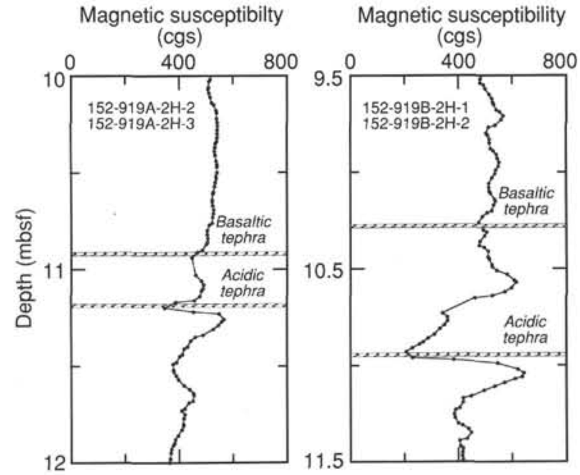

Figure 20. Plot of magnetic susceptibility from duplicate cores of the uppermost sediments of Holes 919A and 919B. The lower acidic tephra is characterized by a low susceptibility, presumably as a result of dilution of the sediments with low-iron acidic glass. The basaltic tephra, of similar thickness, was not recognized in the MST data.

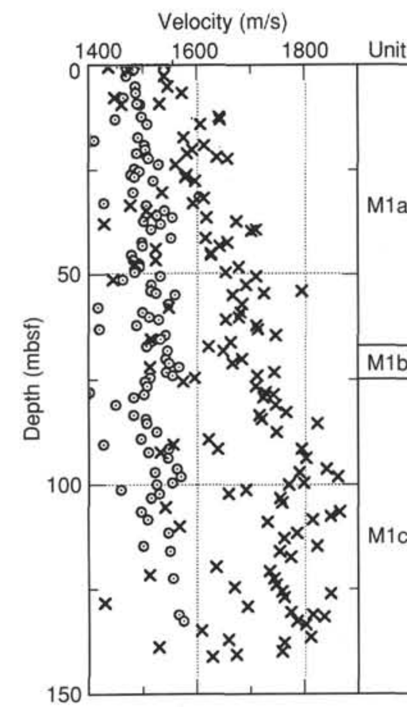

Figure 21. Discrete longitudinal (V_z, circles) and transverse (V_x, crosses) sonic velocities for sediments recovered at Site 917. Note the increase in the difference (acoustic anisotropy) between V_z and V_x with depth.

Undrained Shear Strength

Owing to equipment failure, no shear strength vane values were obtained at Site 919.

Table 9. Tabulation of thermal conductivity measurements for Holes 919A and 919B.

Core, section, interval (cm)	Depth (mbsf)	Thermal conductivity (W/[m·K])
152-919A-		
1H-1, 60	0.60	0.902
1H-3, 60	3.60	0.974
1H-5, 60	6.60	0.858
2H-1, 60	8.60	1.058
2H-3, 60	11.60	1.051
2H-5, 60	14.60	1.009
4H-6, 60	35.10	1.400
5H-6, 60	44.60	1.231
6H-6, 60	54.10	1.049
7H-5, 60	62.10	1.112
8H-5, 60	71.60	1.295
9H-6, 60	82.60	1.275
10H-3, 60	87.60	1.096
152-919B-		
1H-6, 60	8.10	0.955
2H-2, 60	11.30	0.989
2H-4, 60	14.30	0.978
2H-6, 60	17.30	1.023
3H-1, 60	90.60	0.925
3H-3, 60	93.60	1.276
3H-6, 70	98.20	1.062
4H-1, 60	100.10	1.184
4H-3, 60	103.10	1.003
4H-5, 60	106.10	1.306
5H-1, 60	109.60	1.213
5H-3, 60	112.60	1.087
5H-5, 60	115.60	1.138
6H-1, 60	119.10	1.330
6H-3, 60	122.10	1.234
6H-5, 60	125.10	1.153
7H-1, 60	128.60	1.017
7H-3, 60	131.60	1.186
7H-5, 60	134.60	1.399
8H-1, 60	138.00	1.044

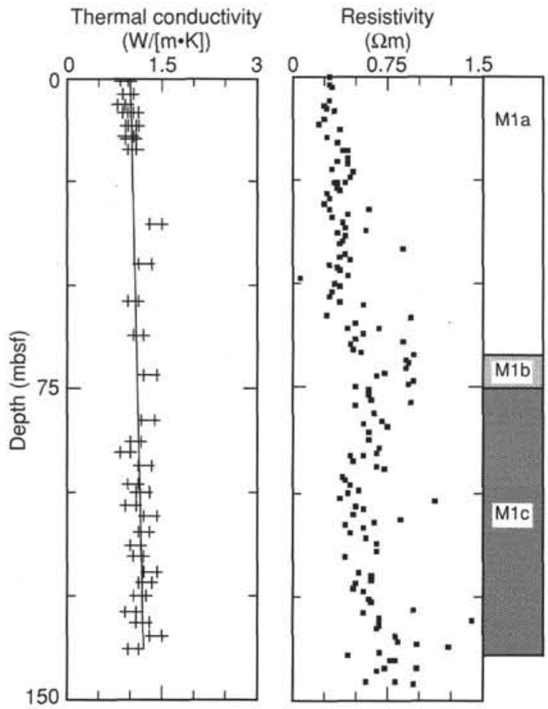

Figure 22. Thermal conductivity and electrical resistivity data for Site 919.

Thermal Conductivity and Electrical Resistivity

Thermal conductivities for Site 919 are listed in Table 9 and illustrated in Figure 22. Full-space measurements were performed for two to three sections per core. Thermal conductivity values for Site 919 show little variation and generally are within experimental error of a linear increase from 1.0 W/(m·K) at the surface to 1.4 W/(m·K) at the bottom of Hole 919B.

Electrical resistance was measured for each section for Holes 919A and 919B. Resistivity was calculated and is tabulated in Table 10 and illustrated in Figure 22. Resistivity increases linearly with depth from 0.3 Ωm at the seafloor to 0.8 Ωm at the bottom of Hole 919B. At 65 mbsf, a break was seen in resistivity that correlates with breaks observed in the porosity and *P*-wave velocity records (top of Subunit M1b). This confirms that both velocity and resistivity depend upon the porosity (and hence, the water content) of the sediment. The lower the porosity (and the water content), the higher the acoustic velocity and the higher the resistivity of the sediment.

Summary

On the basis of the physical properties measurements performed at Site 919, we suggest that the recovered Pliocene–Pleistocene sediments have similar physical properties. The division of the sediments into three mechanical subunits (M1a, M1b, and M1c) within a single mechanical Unit M1 reflects this similarity and agrees with the single lithologic unit established in the "Lithostratigraphy" section (this chapter).

Ms 152IR-112

NOTE: For all sites drilled, core-description forms ("barrel sheets") can be found in Section 4, beginning on page 303. Forms containing smear-slide data can be found in Section 5, beginning on page 925. GRAPE, Index property, MAGSUS and Natural gamma-ray data are presented on CD-ROM (back pocket).

Table 10. Electrical resistivity measurements for Holes 919A and 919B.

Core, section, interval (cm)	Depth (mbsf)	Resistance (Ω)	Resistivity (Ωm)
152-919A-			
1H-1, 30	0.30	14.00	0.299
1H-2, 42	1.92	13.00	0.298
1H-2, 122	2.72	15.00	0.321
1H-4, 121	5.71	13.30	0.285
1H-5, 120	7.20	11.40	0.244
1H-6, 35	7.85	12.60	0.269
2H-1, 39	8.39	15.60	0.334
2H-2, 45	9.95	11.30	0.242
23H-3, 3	11.33	10.10	0.216
2H-4, 35	12.85	17.40	0.373
2H-5, 97	14.97	12.30	0.263
2H-6, 62	16.12	16.60	0.356
3H-1, 32	17.82	20.50	0.439
3H-1, 33	17.83	18.80	0.403
3H-2, 97	19.97	20.10	0.431
3H-3, 64	21.14	20.60	0.441
3H-3, 15	20.65	16.40	0.351
3H-4, 102	23.02	22.30	0.477
3H-4, 3	22.33	14.30	0.306
3H-5, 72	24.22	21.00	0.449
3H-6, 74	25.74	19.40	0.415
3H-6, 24	25.24	15.60	0.334
3H-6, 83	25.83	16.10	0.344
3H-7, 21	26.71	16.20	0.346
4H-1, 20	27.20	18.00	0.385
4H-1, 111	28.11	12.90	0.276
4H-2, 80	29.30	13.80	0.295
4H-3, 90	30.90	11.50	0.246
4H-4, 37	31.87	28.00	0.599
4H-4, 74	32.24	13.90	0.297
4H-5, 41	33.41	20.80	0.445
4H-5, 94	33.94	15.10	0.323
4H-6, 65	35.15	19.00	0.406
4H-7, 33	36.33	19.40	0.415
5H-1, 33	36.83	27.50	0.589
5H-1, 121	37.71	17.00	0.364
5H-2, 32	38.32	19.10	0.409
5H-3, 22	39.72	18.30	0.391
5H-3, 91	40.41	17.70	0.379
5H-4, 73	41.73	40.80	0.873
5H-5, 28	42.78	19.60	0.419
5H-5, 100	43.50	18.00	0.385
5H-6, 27	44.27	21.40	0.458
5H-6, 123	45.23	13.30	0.284
5H-7, 20	45.70	16.20	0.346
6H-1, 92	46.92	17.20	0.368
6H-2, 34	47.84	20.00	0.428
6H-2, 108	48.58	2.900	0.0621
6H-3, 81	49.81	15.60	0.334
6H-4, 17	50.67	17.90	0.383
6H-4, 97	51.47	14.50	0.310
6H-5, 73	52.73	13.80	0.295
6H-6, 64	54.14	18.00	0.385
6H-6, 127	54.77	26.30	0.563
6H-7, 14	55.14	26.40	0.565
7H-2, 37	57.37	12.90	0.276
7H-2, 102	58.02	43.80	0.938
7H-3, 66	59.16	23.50	0.503
7H-4, 44	60.44	32.60	0.698
7H-4, 90	60.90	20.00	0.428
7H-5, 70	62.20	26.50	0.567
7H-6, 18	63.18	23.20	0.496
7H-6, 88	63.88	41.30	0.884
7H-7, 18	64.68	21.60	0.462
8H-1, 60	65.60	22.00	0.471
8H-1, 126	66.26	25.00	0.535
8H-2, 76	67.26	45.00	0.963
8H-3, 30	68.30	42.00	0.899
8H-3, 110	69.10	43.00	0.921
8H-4, 75	70.25	41.50	0.888
8H-5, 24	71.24	34.00	0.728
8H-5, 116	72.16	31.00	0.663
8H-6, 84	73.34	45.00	0.963
8H-7, 25	74.25	43.00	0.921
9H-1, 25	74.75	23.20	0.496
9H-1, 112	75.62	28.00	0.599
9H-2, 82	76.82	27.80	0.595
9H-3, 66	78.16	29.00	0.621
9H-3, 125	78.75	43.90	0.940
9H-4, 48	79.48	23.70	0.507
9H-5, 69	81.19	30.40	0.651
9H-6, 88	82.88	32.80	0.702
9H-7, 16	83.66	25.90	0.554
10H-1, 53	84.53	34.80	0.745
10H-2, 10	85.60	28.20	0.604
10H-3, 66	87.66	28.60	0.612
10H-4, 75	89.25	32.20	0.689
10H-5, 60	90.60	30.78	0.659
10H-6, 12	91.62	26.30	0.563
152-919B-			
3H-2, 12	91.62	21.00	0.449
3H-2, 89	92.39	22.70	0.486
3H-3, 70	93.70	31.20	0.668
3H-4, 28	94.78	33.80	0.723
3H-5, 29	96.29	18.60	0.398
3H-5, 112	97.12	19.40	0.415
3H-6, 65	98.15	21.90	0.469
3H-7, 61	99.61	24.10	0.516
4H-1, 51	100.01	20.50	0.439
4H-2, 27	101.27	17.70	0.379
4H-2, 128	102.28	52.30	1.120
4H-3, 71	103.21	23.40	0.501
4H-4, 16	104.16	26.00	0.556
4H-4, 129	105.29	22.40	0.479
4H-5, 83	106.33	40.20	0.861
4H-6, 38	107.38	30.20	0.646
4H-6, 119	108.19	19.40	0.415
4H-7, 22	108.72	26.20	0.561
5H-1, 84	109.84	21.70	0.464
5H-2, 84	111.34	26.90	0.576
5H-3, 61	112.61	30.90	0.661
5H-4, 70	114.20	31.30	0.670
5H-5, 48	115.48	19.80	0.424
6H-1, 82	119.32	24.60	0.526
6H-2, 34	120.34	28.80	0.616
6H-2, 124	121.24	29.70	0.636
6H-3, 61	122.11	23.80	0.509
6H-4, 50	123.50	22.30	0.477
6H-4, 112	124.12	26.20	0.561
6H-5, 123	125.73	27.90	0.597
6H-6, 51	126.51	29.50	0.631
6H-7, 51	128.01	45.00	0.963
7H-2, 4	130.04	31.80	0.681
7H-2, 126	130.76	66.00	1.413
7H-3, 24	131.24	32.60	0.698
7H-3, 118	132.18	32.00	0.685
7H-4, 54	133.04	31.20	0.668
7H-5, 51	134.51	38.00	0.813
7H-6, 49	135.99	39.00	0.835
7H-6, 115	136.65	46.00	0.985
7H-7, 46	137.46	57.00	1.220
8H-1, 80	138.30	31.80	0.681
8H-2, 38	139.38	20.20	0.432
8H-2, 115	140.15	37.50	0.803
8H-3, 13	140.63	36.00	0.771
8H-4, 25	142.25	34.20	0.732
8H-4, 68	142.68	45.60	0.976
8H-4, 132	143.32	31.10	0.666
8H-6, 25	145.25	27.10	0.580
8H-6, 68	145.68	38.20	0.818
8H-6, 132	146.32	45.00	0.964